The Fifth Generation Regional Climate Modeling System, RegCM5: the first CP European wide simulation and validation over the CORDEX-CORE domains.

Coppola Erika [1], Filippo Giorgi[1], Graziano Giuliani[1], Emanuela Pichelli[1], James M. Ciarlo`[1,5], Francesca Raffaele[1], Rita Nogherotto[1,7], Michelle Simões Reboita[1,2], Chen Lu[1], Natalia Zazulie[1,3], Luiza Vargas-Heinz[1,4], Andressa Andrade Cardoso[1,6], Johannes de Leeuw[1,7]

[1]The Abdus Salam International Centre for Theoretical Physics, Trieste, Italy
[2]Federal University of Itajubá, Itajubá-MG, Brazil
[3]National Council of Scientific and Technical Research (CONICET), Buenos Aires, Argentina
[4]Università degli Studi di Trieste, Trieste, Italy
[5]University of Malta, Malta
[6]Departamento de Ciências Atmosféricas, Instituto de Astronomia, Geofísica e Ciências Atmosféricas, Universidade de São Paulo, Rua do Matão 1226, Cidade Universitária, São Paulo,SP,Brazil.
[7]The National Institute of Oceanography and Applied Geophysics, Trieste, Italy.

Abstract

The Regional Climate Modeling system (RegCM) has undergone a significant evolution over the years, leading for example to the widely used versions RegCM4 and RegCM4-NH. In response to the demand for higher resolution, a new version of the system has been developed, RegCM5, incorporating the non-hydrostatic dynamical core of the MOLOCH weather prediction model. In this paper we assess the RegCM5's performance for 9 CORDEX-CORE domains, including a pan-European domain at convection-permitting resolution.

We find temperature biases generally in the range of -2 to 2 degrees Celsius, higher in the northernmost regions of North America and Asia during winter, linked to cloud water overestimation. Central Asia and the Tibetan Plateau show cold biases, possibly due to sparse station coverage. The model exhibits a prevailing cold bias in maximum temperature and warm bias in minimum temperature, associated with a systematic overestimation of lower-level cloud fraction, especially in winter.

Taylor diagrams indicate a high spatial temperature pattern correlation with ERA5 and CRU data, except in South America and the Caribbean region. The precipitation evaluation shows an overestimation in South America, East Asia, and Africa. RegCM5 improves the daily precipitation distribution compared to RegCM4, particularly at high intensities. The analysis of wind fields confirms the model's ability to simulate monsoon circulations. The assessment of tropical cyclone tracks highlights a strong sensitivity to the tracking algorithms, thus necessitating a careful model interpretation.

Over the European region, the convection permitting simulations especially improve the diurnal cycle of precipitation and the hourly precipitation intensities.

Introduction

Since the initial work of Dickinson et al. (1989) and Giorgi and Bates (1989) introducing the first version of the Regional Climate Modeling system (RegCM1), the dynamical downscaling technique using limited-area Regional Climate Models (RCMs) has become a well-known method used worldwide (Giorgi 2009). The RCM community has witnessed the evolution of various RCM systems, including subsequent model versions of the RegCM framework: RegCM2, RegCM2.5, RegCM3, and the latest RegCM4 (Giorgi et al., 1993a, b; Giorgi and Mearns, 1999; Pal et al., 2007; Giorgi et al., 2012). These model developments largely stemmed from the incorporation of new and more advanced physics packages, with the exception of the RegCM1 to RegCM2 transition, which brought an update to the model's dynamical core, adopting the MM5's hydrostatic dynamical representation (Grell et al., 1994).

RegCM4, in particular, has emerged as a cornerstone in the field, finding extensive use in a diverse range of projects and applications, from process studies to paleo and future climate projections. This includes participation in the Coordinated Regional Downscaling Experiment (CORDEX, Giorgi et al., 2009; Gutowski et al., 2016). RegCM4 is designed to be coupled with ocean, land, chemistry, and aerosol modules in a fully interactive way, adding to its versatility (Sitz et al., 2017).

However, as the demand for higher resolutions escalates, with the RCM community increasingly reaching "convection-permitting" resolutions of a few kilometers, RegCM4's hydrostatic dynamical core has been recognized as a limiting factor for such applications. As a result, the RegCM4 dynamical core underwent a significant upgrade, including the MM5 non-hydrostatic dynamics and leading to the development of RegCM4-NH (Coppola et al., 2021). RegCM4-NH has already extensively been used for climate simulations at convection-permitting scales, e.g. within the European Climate Prediction System (EUCP) project and the CORDEX Flagship Pilot Study dedicated to convection (CORDEX-FPSCONV) (Coppola et al. 2020). Its potential has been demonstrated through multi-model experiments, including those carried out over the greater Alpine region by Ban et al. (2021) and Pichelli et al. (2021), over the South America region of La Plata basin (Betolli et al., 2021; da Rocha et al., 2023) and the region of Lake Victoria in Africa (Lipzig et al., 2023; Glazer et al. 2023).

One of the major drawbacks of the RegCM4-NH is the computational cost to run the model, since the MM5 dynamical core is still based on a split explicit scheme requiring short time steps for stability constraints. In addition, the MM5 scheme includes a relatively high diffusion term, also to increase stability. For this reason, a new version of the RegCM modeling system, RegCM5 was developed by incorporating the dynamical core of the non-hydrostatic weather prediction model MOLOCH (Buzzi et al., 2014; Malguzzi et al., 2006; Trini Castelli et al., 2020) as part of a collaborative effort between the ICTP RegCM modeling team and the Institute of Atmospheric Sciences and Climate (ISAC) of the National Research Council (CNR) of Italy. The first version RegCM5 was introduced by Giorgi et al. (2023), who tested it at convection parametrized and convection permitting resolutions over the Euro-CORDEX domain and the CORDEX FPS convection Alpine domain. In these experiments, not only the model was 4-5 times more computationally efficient than the old RegCM4 and RegCM4-NH counterparts, but also improved different aspects of model performance, and in particular the occurrence of extreme precipitation events and some systematic temperature biases (Giorgi et al. 2023).

RegCM5 thus represents an important step forwards for model users, in particular when using the model at very high resolutions. It is important to acknowledge that the success of the RegCM system is not only the work of the core development teams, but also a result of contributions from the broader user community, who play a vital role in testing the model, identifying errors, customizing model configurations, and implementing new components. As RegCM5 has become available for public use, ongoing feedback and optimization efforts from prospective users will continue to refine the model's performance and applicability. This is especially important in view of the fact that the RegCM system includes multiple representations of different physics processes, which can be quite sensitive to the region of application.

For this reason, it is very helpful to provide model users with some basic information of the performance of a standard version of the model optimized over a variety of climatic settings, which can then provide the basis of more detailed customizations for different applications. Therefore, in this paper we extend the analysis of Giorgi et al. (2023) by presenting a version of the model optimized and tested over nine domains used in the CORDEX-CORE effort (Giorgi et al. 2021; Teichman et al, 2020; Coppola et al., 2020), along with a convection-permitting experiment covering for the first time the entire European region. A number of different aspects of model performance are assessed using a variety of observation datasets for model validation, and for all experiments the model is driven at the lateral boundaries by reanalyses of observations.

We first present in section 2 a brief summary of the main model features, the methodology and setting for the simulations reported in section 3, results are discussed in section 4 and summary and future outlooks are provided in section 5.

RegCM5 model description

RegCM5 includes both hydrostatic and non-hydrostatic dynamical cores, as well as a wide range of physics options. It can be employed as a limited area model for any region globally or using a tropical band configuration (Coppola et al., 2012). The significant enhancement in RegCM5 compared to the previous version RegCM4 is the integration of the non-hydrostatic dynamical core from the MOLOCH weather prediction model, along with some upgrades to the model physics.

The MOLOCH dynamical core used in RegCM5 is described by Giorgi et al. (2023) and references therein. It uses a hybrid terrain-following uniform vertical coordinate and an Arakawa and Lamb C horizontal grid with uniform spacing and staggered wind components.

The model equations are expressed in terms of the variables $(T, P, \Pi, \Theta, u, v, w, q, T_v)$, where

- T is the temperature
- P is the pressure
- q_v, q_c, q_i are the mass mixing ratio of water vapor, liquid water and ice water
- $\Pi = \left(\frac{P}{P_0}\right)^{\frac{R_d}{C_{p_d}}}$ is the Exner function

- $\Theta_v = \frac{T_v}{\Pi}$ is the virtual potential temperature and
- $T_v \approx T(1 + 0.61q_v - q_c - q_i)$ is the virtual temperature

The prognostic equations for Π and Θ_v are a good approximation of the exact thermodynamic and continuity equation of moist air. The horizontal and vertical derivatives are computed using a second order, centered finite difference scheme, while the time integration follows a three-step explicit scheme: vertical sound wave propagation with an implicit Euler-backward scheme with time step dt_s, advection terms with a second-order total variation method with time step dt_a, and physical parameterization terms added with a user-configured large time step dt_p. The dt_a and dt_s time steps are integer fractions of dt_p, i.e.

$$dt_a = \frac{dt_p}{n_{adv}}, dt_s = \frac{dt_a}{n_{sound}}$$

with n_{sound} and n_{adv} being user configurable parameters. The generalized vertical velocity is zero at the surface and at the model top. No explicit diffusion is required and numerical stability is attained by applying a second order spatial filter on the divergence of the horizontal wind with a user configurable coefficient.

For further technical details we refer to Giorgi et al. (2023) and Malguzzi et al. (2006) who provide comprehensive information on the model equations and solution procedures.
A summary of the additional features available in the new RegCM5 model version optimized over the CORDEX-CORE domains is reported in Table 1.

Table 1: Dynamics, Physics and Coupled Component Options Available in RegCM5.
Note. Bold letters highlight the options newly available since the RegCM5 version described by Giorgi et al. (2023).

Model aspects	**Available options**
Dynamics	• Hydrostatic, vertical pressure coordinate (Giorgi et al, 1993a) • Non-hydrostatic, vertical pressure coordinate (Coppola et al, 2012) • Non-hydrostatic, height based coordinate (MOLOCH, Malguzzi et al, 2006, Davolio et al. 2020)
Radiative transfer	• Modified CCM3 (Kiehl et al, 1996) • RRTM (Mlawer et al, 1997a,b)
Planetary Boundary Layer	• Modified Holtslag (Holtslag et al. 1990) • UW-PBL (Bretherton et al. 2004)
Cumulus convection	• Simplified Kuo (Anthes et al. 1987, not available for MOLOCH dynamics) • Grell (Grell 1993) • MIT (Emanuel & Zivkovic-Rothman 1999) • Tiedtke (Tiedtke 1989) • Kain-Fritsch (Kain 2004)

Resolved scale precipitation	• SUBEX (Pal et al, 2000) • WRF-single-moment-microphysics classes 5 (Hong, Dudhia and Chen, 2004) • Nogherotto-Tompkins (Nogherotto et al, 2016)
Cloud fraction	• **Sundqvist (Sundqvist, 1988)** • **Xu-Randall (1996)** • **Both modified according to Liang et al. (2005)**
Land Surface	• BATS (Dickinson et al. 1993) • CLM3.5 (Steiner et al. 2009) • CLM4.5 (Oleson et al, 2013) • Sub-grid BATS (Giorgi et al. 2003) and CLM4.5
Land Use	• **Dynamical land use forcing from LUCAS LUC V1.1, based on LUH2 (Hoffmann et al. 2023) for the European Domain**
Ocean fluxes	• BATS (Dickinson et al. 1993) • Zeng (Zeng et al. 1998) • COARE (Fairall et al., 2003) • Diurnal sea surface temperature (Zeng & Beljaars 2005)
Interactive aerosols	• Organic and black carbon, SO4 (Solmon et al. 2006) • Dust (Zakey et al. 2006) • Sea salt (Zakey et al. 2008) • Gas-phase (Shalaby et al, 2012) • Pollen (Liu et al, 2016) • **Implementation of Global Aerosol OPP Profile Reanalysis from MERRA-2 (Gelaro et al. 2017, last version available at: DOI:** 10.34730/bc801a23b8bf48e98a50e23e909bf19c **), but only with one optical band (visible)**
Interactive lake	• 1D diffusion/convection (Hostetler et al. 1993)
Interactive vegetation	• CLM4.5 CNDV (Shi et al, 2018)
Tropical band	• (Coppola et al 2012)

Coupling	• RegCM-ES (Sitz et al. 2017)
	  ○ ROMS Ocean (Ratnam et al, 2009)
	  ○ MIT GCM Ocean (Artale et al. 2010)
	  ○ ChyM hydrology (Di Sante et al, 2019)
	  ○ BFM biogeochemical (Reale et al, 2020)

Sea ice	• BATS (Dickinson et al. 1993)

IPCC forcing	● AR4 GHG (CMIP3 : A1B, A2, B1, B2) ● AR5 GHG (CMIP5 : RPC2.6, RCP4.5, RCP6.0, RCP8.5) ● AR6 GHG (CMIP6 : SSP119, SSP126, SSP245, SSP370, SSP434, SSP460, SSP534, SSP585) ● SPARC SOLARIS HEPPA irradiances ● SPARC CCMI Ozone ● Anthropogenic Aerosol Simple Plume model

Methods

The RegCM5 model has been tested over the entire set of CORDEX-CORE domains, which were previously simulated with the RegCM4.7 version (Coppola et al., 2020; Giorgi et al., 2021). Additionally, the model was tested for the first time at a convection-permitting resolution over a pan-European domain. For each domain, multiple observations and reanalysis data have been utilized for model assessment, as reported in Table 2.

Table 2: Observational Datasets.

Observed Datasets	Domain	Variables	Data type	Spatial Resolution	Temporal Resolution	Period	Reference
CPC_Global	Global Land	PRECIP TMAX TMIN	Gridded, Station based	0.50 degrees	DAILY	1979-2021	Chen et al. (2008)
TRMM	Tropics	PRECIP	Satellite observation based	0.25 degrees	3-HOURLY	1998-2017	Kummerow et al. (1998)
MSWEP	Global	PRECIP	Derived by optimally merging a range of gauge, satellite, and reanalysis estimates	0.10 degrees	DAILY	1979-2020	Beck et al. (2019)
GPCP	Global	PRECIP	Satellite observation based	0.25 degrees	DAILY	1979-2009	Adler et al. (2003)
CRU	Global Land	PRECIP TMEAN	Station based	0.50 degrees	MONTHLY	1901-2015	Harris et al. (2020)
APHRO	India and East Asia	PRECIP	Grid	0.25 degrees	DAILY	1951-2007	Yatagai et al. (2009)
E_OBS	Europe Land	PRECIP TMAX TMIN	Grid	0.25 degrees	DAILY	1950-2015	Cornes et al. (2018)

CN05.1	China	PRECIP TMEAN	Station based	0.25 degrees	DAILY	1961-2012	Wu & Gao (2013)
ERA5	Global	WIND, PRECIP, CLOUD FRACTION, CLOUD WATER, CLOUD ICE, MEAN SEA LEVEL PRESSURE, TMEAN	Reanalysis	0.25 degrees	HOURLY	1940-Present	Hersbach et al. (2020)
IBTrACS	Global	TROPICAL CYCLONES TRACK	Merging datasets from different agencies	-	DAILY	1842-Present	Knapp et al. (2010, 2018)
REGNIE	Germany	PRECIP	Station based	1 km	DAILY	1961-2014	Rauthe et al., 2013
RADKLIM	Germany	PRECIP	Radar based (rain gauges calibration)	1 km	HOURLY	2001-2009	Kreklo et al. (2020)
SPAIN02	Spain	PRECIP	Station based	0.11 degrees	DAILY	1971-2010	Herrera et al., 2010
CARPATCLIM	Carpatians	PRECIP	Station based	0.1 degrees	DAILY	1961-2010	Szalai et al. (2013)
ENG_REGR	Great Britain	PRECIP	Station based	5 km	DAILY	1990-2010	http://www.precisrcm.com/Erasmo/ncic.uk.11.tgz
COMEPHORE	France	PRECIP	Reanalysis based on radar and rain gauges	1 km	HOURLY	1997-2017	Tabary et al. (2012)
GRIPHO	Italy	PRECIP	Station based gridded dataset	3 km	HOURLY	2001-2016	Fantini (2019)
EURO4M	Alps	PRECIP	Station based gridded dataset	5 km	DAILY	1971-2008	Isotta et al. (2014)
PTHBV	Sweden	PRECIP	Station based gridded dataset	4 km	DAILY	1961-2011	https://opendata-download-metanalys.smhi.se Johansson (2000)
METNO	Norway	PRECIP	Station based gridded dataset	1 km	DAILY	1980-2008	Mohr et al. (2009)

RdisaggH	Switzerland	PRECIP	Combination of rain-gauge data and radar measurements	1 km	HOURLY	2003-2010	Wüest et al. (2010)
CEH-GEAR	Great Britain	PRECIP	Rain-gauge based gridded dataset	1 km	HOURLY	1990-2016	Lewis et al. (2022)

All simulations use ERA5 reanalysis fields (Hersbach et al., 2020) as initial and lateral boundary conditions. Specific model configurations for each domain, including spatial resolution and the simulation period, are provided in Table 3.

Table 3: Model configuration for each domain.

DOMAIN	**Period**	**Horizontal Resolution**	**Vertical Resolution**	**Boundary Layer Scheme** (ib ltyp)	**Cumulus convection scheme** (icup_lnd/ocn)	**Moisture scheme** (ipptis)	**Cloud fraction algorithm** (icldfrac)	**Dynamical Land Use**
Australasia	2000-2009	25 km	30 levels	Holtslag PBL	Tiedtke/ Tiedtke	Explicit moisture Nogherotto/ Tompkins	SUBEX	NO
East Asia	2000-2009	25 km	30 levels	Holtslag PBL	Tiedtke/ Tiedtke	Explicit moisture Nogherotto/Tompkins	Xu-Randall empirical	NO
South East Asia	2000-2009	25 km	30 levels	Holtslag PBL	Tiedtke/ Tiedtke	Explicit moisture Nogherotto/Tompkins	SUBEX	NO
South America	2000-2009	25 km	30 levels	Holtslag PBL	Tiedtke/ Tiedtke	Explicit moisture Nogherotto/Tompkins	SUBEX	NO
Central America	2000-2009	25 km	30 levels	Holtslag PBL	Tiedtke/ Tiedtke	Explicit moisture Nogherotto/Tompkins	SUBEX	NO
Europe	2000-2004	3 km	30 levels	Holtslag PBL	Tiedtke/ Tiedtke	Explicit moisture Nogherotto/Tompkins	Xu-Randall empirical	NO
	1980-2010	12 km	30 levels	Holtslag PBL	Tiedtke/ Tiedtke	Explicit moisture Nogherotto/Tompkins	Xu-Randall empirical	YES

South Asia	2000-2009	25 km	30 levels	Holtslag PBL	Tiedtke/ Tiedtke	Explicit moisture Nogherotto/Tompkins	Xu-Randall empirical	NO
North America	2000-2009	25 km	30 levels	Holtslag PBL	Tiedtke/ Tiedtke	Explicit moisture Nogherotto/Tompkins	Xu-Randall empirical	NO
Africa	2000-2009	25 km	30 levels	Holtslag PBL	Tiedtke/ Tiedtke	Explicit moisture Nogherotto/Tompkins	SUBEX	NO

The model validation was conducted over the set of sub-regions identified in the AR6 WGI IPCC report covered by the RegCM5 domains The regions are described by Iturbide et al. (2020). Various metrics were computed to validate the model, encompassing both mean climate and extreme climate distribution, as shown in Table 4.

Table 4: Metrics used for model validation.

Metric	Definition	Unit
T_{mean}	Daily mean 2-m temperature	°C
T_{max}	Daily maximum 2-m temperature	°C
T_{min}	Daily minimum 2-m temperature	°C
pr	Daily/hourly total precipitation	mm/day, mm/hr
pr-frq	Total number of wet days/hours (i.e., days with total precipitation greater than 1 mm)	day/year
pr-int	Average amount of wet-day precipitation	mm/day, mm/hr
p99	The 99th percentile of the precipitation distribution over the time period considered	mm/day, mm/hr
p99.9	The 99.9th percentile of the precipitation distribution over the time period considered	mm/day, mm/hr
cl	Cloud Fraction	%

clw	Cloud Liquid Water	mg/kg
cli	Cloud Ice	mg/kg

Mean seasonal bias

The mean seasonal bias for 2 meter, mean, maximum and minimum temperature (T_{mean}, T_{max}, and T_{min} respectively), mean precipitation (pr), precipitation intensity and frequency (pr-int and pr-frq), as well as the annual total precipitation above the 99th percentile (p99), were used for the validation of the model mean climatology (definition of the metrics can be found in Table 4). For temperature, the model results are compared with observations from the Climate Research Unit (CRU) dataset. For mean precipitation, the reference dataset is the Global Precipitation Climatology Centre (GPCC), and for precipitation intensity/frequency and p99, is the Climate Prediction Center (CPC) one. The seasonal means are first calculated over the baseline period (1980 to 2010 for Europe and 2000 to 2009 for all other domains) at the original resolutions and are subsequently interpolated (distance-weighted average for temperature, and nearest neighbour for precipitation and related metrics) to the resolution of the observations. The area-weighted averages of all variables are then computed over the AR6 WGI IPCC regions contained within each domain, and the biases are then derived by taking the difference between the simulated and observed values. The global bias is obtained in the same way, except that the area-weighted average is calculated over all grids of all domains.

Precipitation distribution

Boxplots were computed for daily precipitation in all regions considered, from RegCM4, RegCM5 and observations. We use the station-based data from CPCexcept for Europe, for which the observation dataset is E-OBS. Due to the steepness of the distribution, the box plots include the 5th and 95th and 99th percentiles.
Note that over some regions, and particularly the Mediterranean, RegCM4 exhibited a notable overestimation of extreme events due to the occurrence of numerical point storms, a problem that is considerably improved in RegCM5. Therefore, in the box plots, events with excessively large amounts in RegCM4 were excluded by adjusting the plot to align with the distribution from observations and RegCM5.

Hourly precipitation distributions for the period 2000-2004 were calculated for the RegCM5 CP and 12 km simulation over Europe and compared with high-resolution hourly observations over Italy, Switzerland, Germany, France and Great Britain (see Table 2). Furthermore, results were compared with the ERA5 reanalysis estimates. Distributions are calculated by taking all available time steps and grid points within each dataset considered. Some of the observational datasets did not have observations at the start of the RegCM5 simulations (e.g Switzerland observational dataset starts in 2003). Therefore, in order to consider a consistent time period for the observations and model simulations, we used the first five available years for each of the observational datasets (e.g. Switzerland 2003-2007).

Daily precipitation distributions are calculated for 2000-2004 for the Europe RegCM5 model simulations, ERA5 and all available observations in the simulated region. In addition to the observational datasets mentioned above, daily precipitation estimates from Sweden, Norway, Spain and the Carpatians are also available (see table 2). All the biases were computed interpolating each observational dataset on the model grid.

Precipitation sub daily analysis

Seasonal daily precipitation cycles were computed for Europe, analysing both the 12 km and the 3 km simulations. The comparison was carried out against ERA5 data as well as different sub-regional hourly observation datasets: GRIPHO (Italy), RdisaggH (Switzerland), RADKLIM (Germany), COMEPHORE (France) and CEH-GEAR (Great Britain). Each high-resolution dataset was interpolated on the coarser model grid and the daily cycle was computed spatially averaging only in the region covered by observations.
Precipitation intensity and frequency for the hourly observation and RegCM5 datasets were calculated using hourly minimum precipitation thresholds of 0.1 mm/hr and 0.5 mm/hr in order to investigate the uncertainties in the data at very low intensities, which can strongly influence the biases. Note that the choice of threshold does not influence the p99.9 estimates as the whole distribution (including dry hours) is used to calculate this variable.

Taylor diagram

Taylor diagrams were used to validate the mean seasonal precipitation and temperature against several reference datasets. For precipitation, the model results are compared with ERA5, CRU, MSWEP, CPC, and GPCC. For temperature, ERA5 and CRU are used, except for additional observation datasets for Europe and East Asia. Specifically, for Europe, precipitation and daily mean temperature are compared against E-OBS, while for several subregions of East Asia, they are compared against APHRO and CN05.1. For each subregion, the gridded seasonal averages of the observed and simulated data are used to calculate the area-weighted centered pattern correlation and the ratio between the simulated and observed standard deviations, which are then used to generate the diagrams.

Cloud distributions

Vertical profiles were computed over each region for the mean seasonal cloud fraction, cloud liquid water and cloud ice in June-July-August (JJA) and December-January-February (DJF) using twelve pressure levels: 1000, 925, 850, 700, 600, 500, 400, 300, 250, 200, 150 and 100 hPa.The calculations were done for both RegCM5 and the ERA5 reanalysis data and covered the period 2000-2009 for all domains, except for Europe, for which 1980-2010 was used.

Upper level circulations

Composites of zonal and meridional wind were computed for 3 different pressure levels, i.e., 850, 500, and 250 hPa. RegCM5 includes a function to perform this task, called sigma2p. This function is first executed to interpolate the wind components from the sigma coordinates to pressure levels. Wind at the selected levels is then extracted, and its seasonal means are calculated over the baseline period. Results of different domains are subsequently interpolated onto the grids of the reference dataset, i.e., ERA5, using distance-weighted average mapping. The composite of global wind is then obtained by directly combining the wind of all domains. In cases where there is an overlap between multiple domains, the average is calculated. For ERA5, wind at the three pressure levels averaged over 2000-2009 is used for all domains except for Europe, where the 1980-2010 average is employed. Wind of the reference dataset is then masked with respect to the RegCM composite to facilitate an intuitive comparison between the two.

Tropical and extratropical cyclones

Tropical and extratropical cyclones were tracked in each domain, but a graphical representation was created by combining all domains into a single map. Three different algorithms for identifying and tracking tropical cyclones (Reboita et al., 2010; Fuentes-Franco et al., 2014, 2017; Hodges, 1994, 1995, 1999) were employed, while one algorithm was used for extratropical systems (Reboita et al., 2010).

a) Reboita et al. (2010)'s algorithm

This algorithm identifies and tracks tropical and extratropical cyclones using cyclonic relative vorticity every 6 hours (0000, 0600, 1200, and 1800 UTC). Before applying the algorithm, the horizontal wind components at 925 hPa (zonal and meridional) are interpolated to a grid with a resolution of 1.5º x 1.5º in latitude and longitude. Once the data are provided to the algorithm, relative vorticity is computed and smoothed to reduce noisy features using the Cresmann (1959) method. The algorithm consists of three main steps: (1) initially, in a specific time step of the dataset, it searches for the minimum relative vorticity by comparing each grid point value with those of 24 surrounding points (nearest-neighbour method). A grid point is a cyclone center candidate when a minimum of relative vorticity is found and is smaller or equal to a threshold (defined as -1×10^{-5} s^{-1}); (2) the coordinates of the grid point identified in (1) are located in the follow time step of the dataset to limit the search area to the 24 neighboring grid points; and (3) once two positions are known, the algorithm calculates the displacement velocity of the cyclone center and uses it as an initial estimate (first guess) to locate the cyclone center in the following time step. This procedure continues until the dissipation (cyclolysis) of the cyclone. When cyclolysis occurs, the algorithm returns to the specific time step of the initial identification and searches for other grid points that could be a cyclone center, and all three steps are repeated. After the cyclone position is identified at a given time step, the algorithm performs an interpolation on a high resolution grid to refine the cyclone center searching a new position in a 250 km radius. Only cyclones with lifetime equal to or higher than 24 hours and equal to or lower than 10 days are included in the statistics. It is important to highlight that we will present all synoptic cyclonic systems detected by the algorithm and not only extratropical and tropical cyclones. For selection of a specific cyclone type, the tracking output would need to be used as input to the Cyclone Phase Space (CPS; Hart, 2003), which analyses the vertical structure of the systems.

b) Fuentes-Franco et al. (2014, 2017)' algorithm

This algorithm, named Kyklop (Fuentes-Franco et al., 2017), is configured to work with three variables (near-surface wind speed at 10 m, mean sea level pressure -MSLP-, and sea surface temperature - SST) and with the time frequency and horizontal resolution (see https://github.com/kyklop-climate/kyklop/blob/master/kyklop/kyklop.py) of the NetCDF file provided as input. In this study, 3-hourly data (0000, 0300, 0600, 0900, 1200, 1500, 1800, and 2100 UTC) are used. The Kyklop algorithm has two main procedures: (1) it searches for grid points that are candidates to be a tropical cyclone in all time steps and (2), subsequently performs the matching of grid points to determine the cyclone's trajectory. This logical sequence differs from Reboita et al. (2010) in that, in their approach, once a grid point is identified as a cyclone center candidate, it is tracked until cyclolysis. In (1), for each time step, Kyklop searches grid points that satisfy the following criteria: wind speed >20 m s^{-1}, MSLP <1005 hPa, and SST >25 °C. As these conditions may be satisfied by some neighbouring grid points, the centroid of the area encompassed by these grid points is considered as the center of the tropical cyclone. In (2), for each detected cyclone grid point in a specific time step, its tracking (following positions) is carried out by checking on next time steps if there are grid points that meet the conditions presented in (1) within a radius of 6º × 6º longitude–latitude. These conditions need to persist for at least 24 hours.

c) Hodges (1994, 1995, 1999)' algorithm

Hodges (1994, 1995, 1999) named his algorithm TRACK, which searches for various types of cyclones based on relative vorticity. However, this algorithm can also be configured for identifying only tropical disturbances. In this case, the TRACK uses the zonal and meridional wind components at different vertical levels (10 m, 850, 700, 600, 500 400, 300 and 200 hPa), and at 6-hour intervals (0000, 0006, 1200 and 1800 UTC). The identification of tropical disturbances involves three main steps: (1) pre-processing filtering, (2) tracking performed following Hodges's references, and the (3) post-tracking filtering - an additional procedure integrated within TRACK (Hodge et al., 2017). The data used in this study were first interpolated to a regular grid of 0.25º x 0.25º before being processed by TRACK. In step (1), the algorithm calculates the vertically averaged relative vorticity between 850-600 hPa . Subsequently, a spectral filter (triangular truncation) is applied, retaining wavenumbers between 6 and 63, in order to remove the noise associated with the smallest spatial scales and the large-scale background. In step (2), the nearest-neighbor method is applied to the processed data from step (1) to identify all tropical disturbances (tropical cyclones will be separated from all systems in step 3). Unlike Reboita et al. (2010), TRACK standardizes the relative vorticity field to positive values in both hemispheres, so it identifies the cyclonic disturbances by maxima of relative vorticity, and, in addition, it applies a threshold: candidates for tropical disturbance need to have relative vorticity > 5 x 10^{-6} s^{-1} (in the Southern Hemisphere the field is scaled by -1). The tropical disturbance location is then refined using a B-spline interpolation. Additionally, the algorithm refines the tracks by minimizing a cost function for track smoothness. The final step (3) is post-tracking filtering, selecting only the tropical cyclones from all tracked tropical disturbances. Tropical cyclones are identified based on three parameters describing their structure: presence of coherent vertical symmetry (presence of a maximum of relative vorticity at each vertical level), warm core, and high near-surface wind speeds. These three parameters must be satisfied for at least 2 days, with a minimum of 24 hours over the ocean. To identify the symmetry, the scheme searches the maximum relative vorticity at the vertical levels (850, 700, 600, 500 400, 300 and 200 hPa). The algorithm uses the location of tropical disturbance computed at the 850-600 hPa level as the starting point. and then a circle with a radius of 5º (geodesic) is delimited. The maximum relative vorticity is then searched inside this area, and the location of this maximum is used as reference for the level above and this procedure is repeated until the uppermost level. The warm core is calculated as the difference between the relative vorticity fields at 850 and 200 hPa (at T63 resolution) and must be greater than 6 x 10^{-5} s^{-1} (indicating stronger winds near the surface than at upper levels). Additionally, the 10-m wind speed must be greater than 17.5 m s^{-1} and is searched within a 6° radius from the cyclone center identified using the vorticity average between 850-600 hPa.

All algorithms provide as output the latitude and longitude at each time step of the cyclone's lifecycle and other features such as MSLP, relative vorticity etc., depending on the algorithm. With the tracking information, it is possible to compute the track density, which is the number of cyclones passing by an area of 1° x 1° divided by the area of this box. We compared the RegCM5 performance in reproducing the cyclonic systems against the ERA5 reanalysis when working with the Reboita et al. (2010) algorithm and against the International Best Track Archive for Climate Stewardship (IBTrACS, version v04; Knapp et al. 2010, 2018) for the other algorithms. IBTrACS collects observed tropical cyclone data from 11 agencies around the world covering all major ocean basins and provides 6-hour data of tropical cyclones locations.

Results

CORDEX-CORE domains

The mean regional biases for mean, maximum, and minimum temperature, mean precipitation, precipitation frequency and intensity, and precipitation above the 99th percentile are presented in Figure 1 for all four seasons (DJF, MAM, JJA, and SON) and for each region, as well as for the global average. Mean temperature biases are generally constrained between -2 and 2 degrees, except for the two northernmost regions of the North American continent (NWN and NEN) and the northernmost eastern region of Asia (RFE) in DJF, where a stronger warm bias is evident.

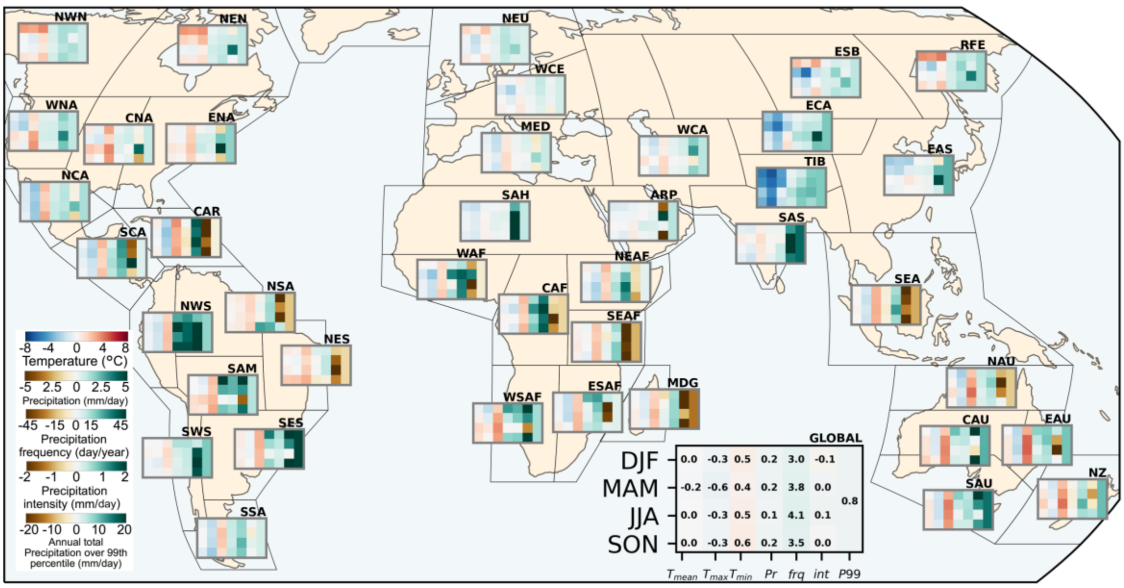

NWN	N.W.North-America	NES	N.E.South-America	CAF	Central-Africa	TIB	Tibetan-Plateau
NEN	N.E.North-America	SAM	South-America-Monsoon	NEAF	N.Eastern-Africa	EAS	E.Asia
WNA	W.North-America	SWS	S.W.South-America	SEAF	So.Eastern-Africa	ARP	Arabian-Peninsula
CNA	C.North-America	SES	S.E.South-America	WSAF	W.Southern-Africa	SAS	S.Asia
ENA	E.North-America	SSA	S.S.South-America	ESAF	E.Southern-Africa	SEA	S.E.Asia
NCA	N.Central-America	NEU	N.Europe	MDG	Madagascar	NAU	N.Australia
SCA	S.Central-America	WCE	Western&Central-Europe	ESB	E.Siberia	CAU	C.Australia
CAR	Caribbean	MED	Mediterranean	RFE	Russian-Far-East	EAU	E.Australia
NWS	N.W.South-America	SAH	Sahara	WCA	W.C.Asia	SAU	S.Australia
NSA	N.South-America	WAF	Western-Africa	ECA	E.C.Asia	NZ	New-Zealand

Figure 1. Mean seasonal bias of each region for Tmean, Tmin, Tmax, pr, pr-frq, pr-int and the annual value of p99. The period covered is 2000-2009, except for the European domain (MED, WCE and NEU regions): 1980-2010. A global mean season bias table with its respective values has been added to the figure.

This is likely due to the overestimation of cloud water for low and middle clouds which increases downward infrared radiation (Figure 2), derived from an excessively stable boundary not well reproduced by the Holtslag PBL scheme (see Table 3), as previously noted in Güttler et al., 2014, or Bae et al., 2023; Gao and Giorgi (2017).

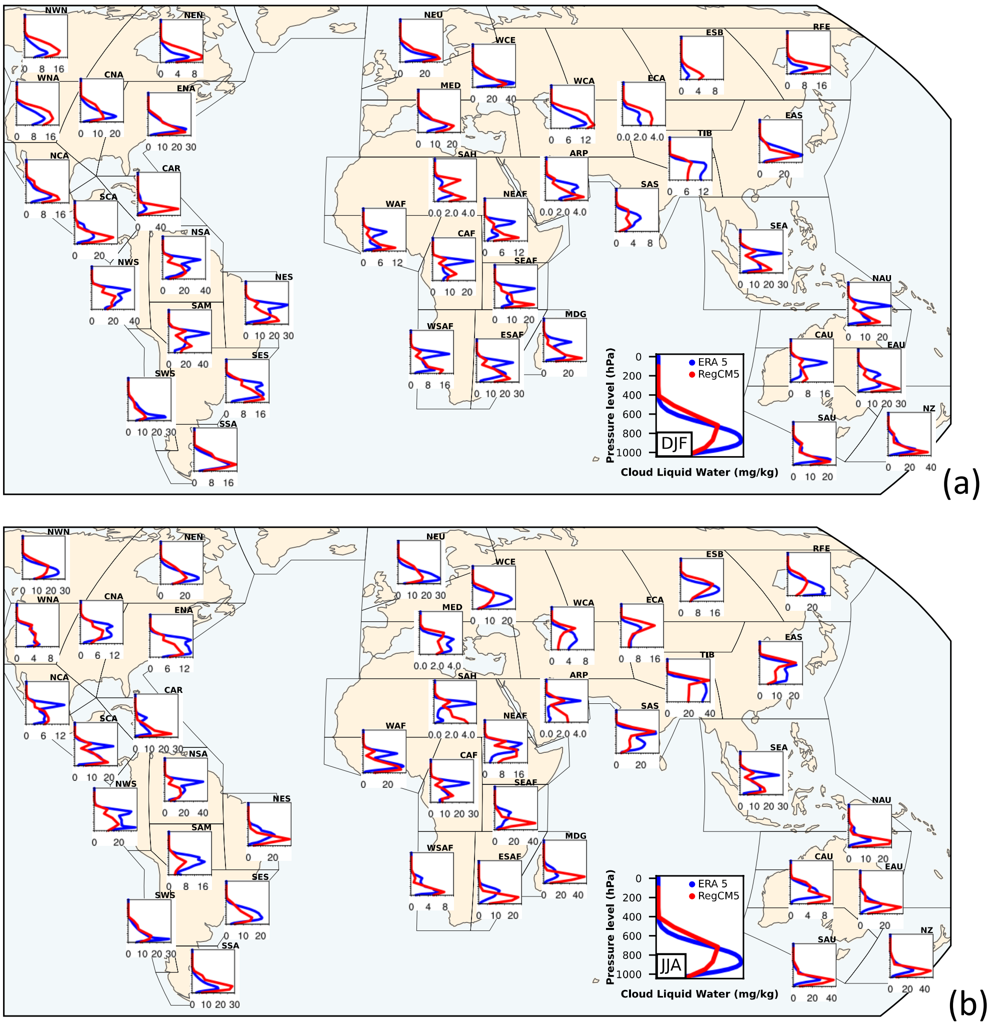

Figure 2. Cloud liquid water vertical profiles for DJF (a) and JJA (b). The period covered is 2000-2009, except for the European domain (MED, WCE and NEU regions): 1980-2010.

Other outlier regions include central Asia, where the Tibetan Plateau is located, showing a cold bias between 3 and 4 degrees in DJF. This is possibly at least partially due to the well-known sparse nature of available stations at high elevations, especially considering that gauge stations are often placed in valleys and only few or none on mountain tops (Xu et al., 2009). Overall, the model has a tendency for a cold bias in maximum (T_{max}) temperature and a warm bias in minimum (T_{min}) temperature across almost all seasons and regions. This tendency is associated with a systematic overestimation of the lower-level cloud fraction (see Figure S1), more pronounced in winter than in summer in both hemispheres but consistently present due to an overestimation of cloud liquid water (Figure 2). In this case, biases are generally within a 2-degree range, except for the warm T_{min} bias in the Caribbean, western South Africa, and

Australasia regions, where the overestimation of the cloud profile is pronounced, and the Tibetan Plateau, showing a cold bias mainly in winter and spring. Cloud ice vertical profiles for DJF and JJA are shown in Figure S2.

In Figure 3a, Taylor diagrams are presented to validate the spatial temperature patterns in each domain and region, considering only land points. The results show for all seasons a strong correlation (0.9 or higher) between the model and the ERA5 and CRU datasets, except for NSA in South America and the Caribbean region (with respect to CRU), where the correlation drops to 0.7. Similar correlations are observed in Central Africa for all seasons except SON and Western Southern Africa for DJF and MAM. Spatial temperature variability is well captured in all regions, with a tendency to overestimate it in South and Central America (mostly in all regions and seasons) and East Asia, where variability is slightly underestimated for the northernmost regions and overestimated for the southern ones. Similar behaviour is observed for maximum and minimum temperature in Figure S3-S4.

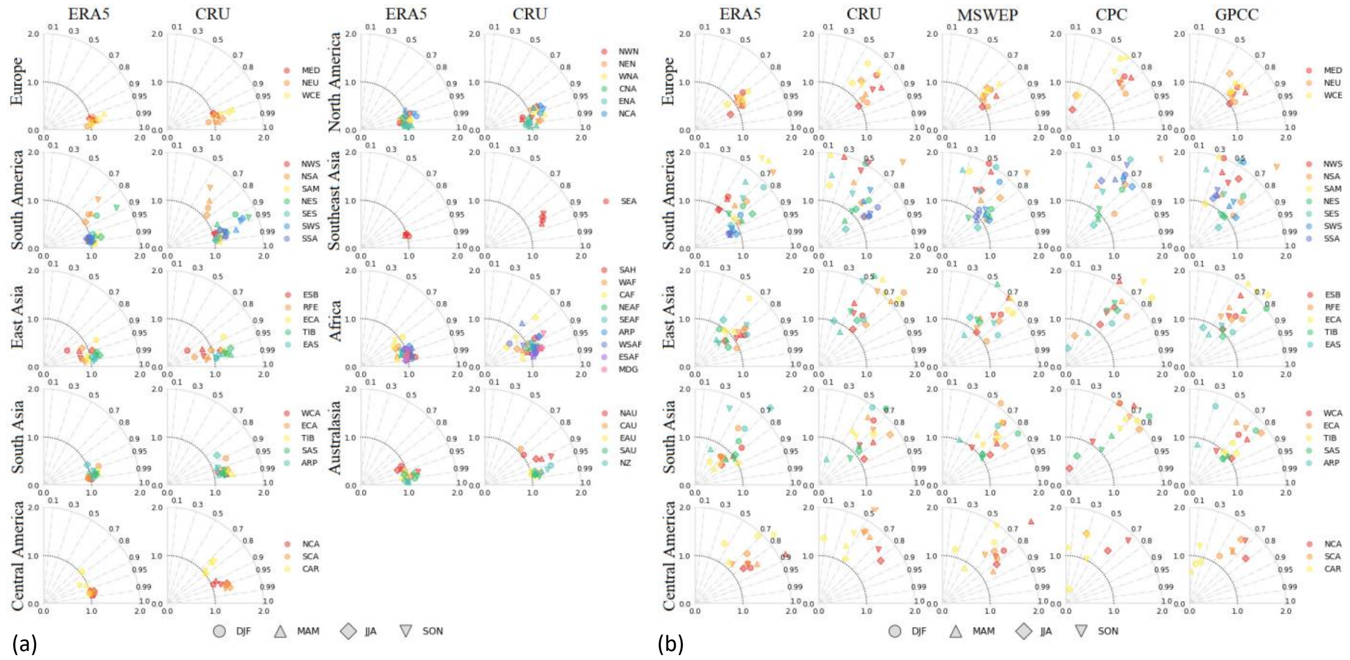

Figure 3. Taylor diagrams for the mean temperature (panel a) and precipitation (panel b) for selected domains. Symbols represent seasons and colors are the subregions of a specific domain.

Taylor diagrams for precipitation are presented in Figure 3b for selected domains and in Figure S5 and S6 for the remaining domains and regional observational datasets. Five different datasets are used for comparison, varying in spatial resolution and origin. Correlation and spatial variability for all domains are in better agreement with the MSWEP and GPCC observational products, which have the highest resolution. Spatial correlation of precipitation ranges between 0.5 and 0.8 in most seasons and regions (Figure 3b and S3) . The model tends to overestimate spatial variability, especially in South America, East Asia, and Africa.

Figure 4 illustrates the comparison of the precipitation intensity distribution in each region between the RegCM5 and RegCM4 models and the observations through box plots. RegCM5 shows a good representation of the precipitation distribution compared to observations and is more realistic than the previous model version, especially for the long tails and most extreme events, where the model strongly ameliorated the problem of numerical point storms found in regCM4.

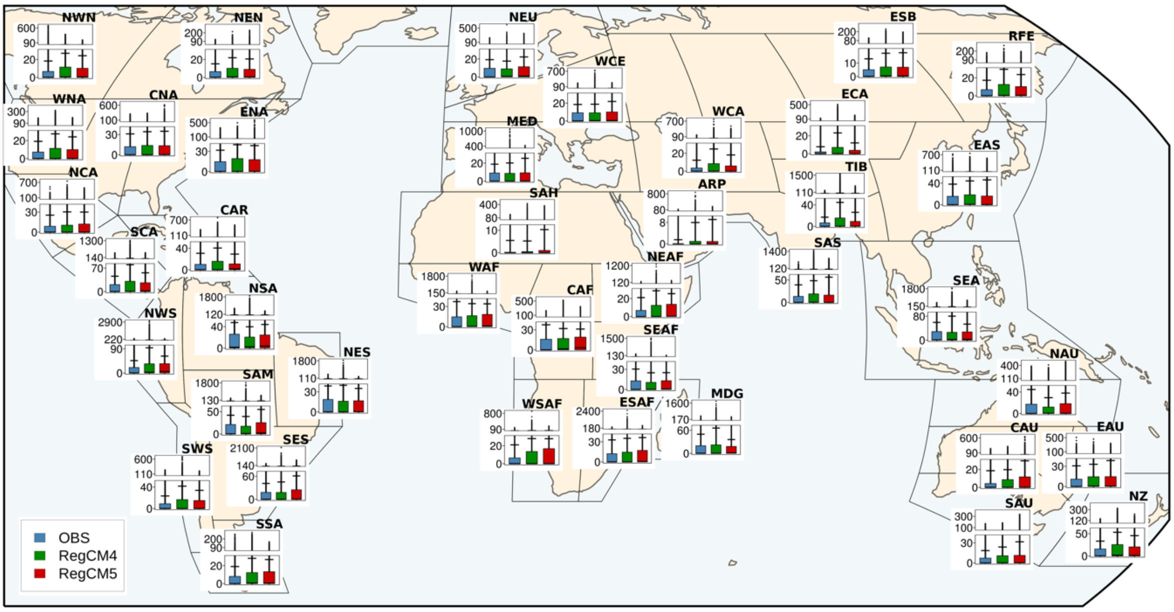

Figure 4. Boxplot of daily precipitation for the period 2000-2009, except for the European domain (MED, WCE and NEU regions): 1980-2010. Colored boxes are limited by the 5th and 95th percentile. The upper black bar indicates the 99th percentile. Blue boxes correspond to the observations from CPC, except for the European domain: EOBS. Green boxes indicate RegCM4 and red boxes, RegCM5. Units are mm per day.

In Figure 5, the 850 hPa wind field is analyzed to validate monsoon circulation in different continents. The model well represents the South Asia monsoon system in terms of intensity and direction of the wind jet. It slightly overestimates the West African monsoon with more inland penetration and a west-east direction compared to observations. The Central America and North America monsoons are well located with correct intensity, while the East Asia monsoon circulation intensity is slightly underestimated . The South America Low-Level Jet (SALLJ) is well reproduced in intensity and direction in the austral summer (DJF), while during JJA the jet intensity over south Bolivia and Paraguay is weaker in the model compared to ERA5. The Caribbean Low-Level Jet is well positioned in both seasons with the right intensity and direction. The wind fields at 500 and 200 hPa are also reported in Figure S7 for completeness.

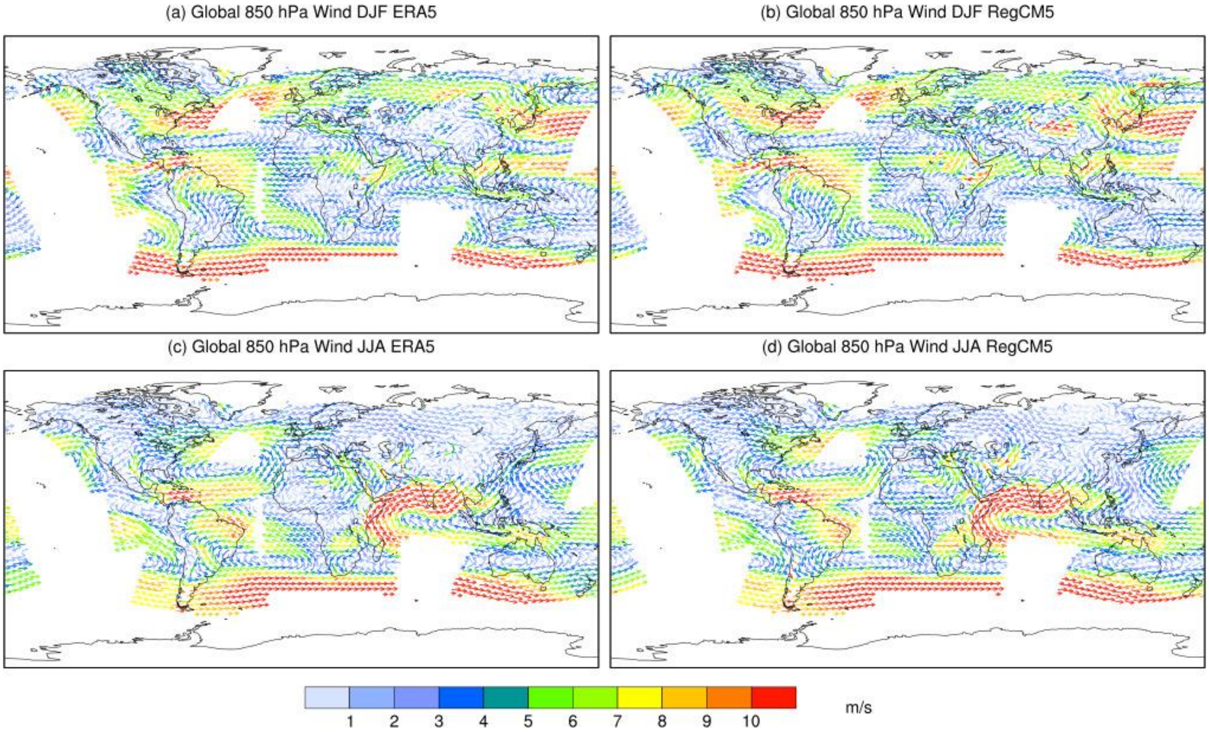

Figure 5. Wind intensity (m/s) and direction (arrows) at 850 hPa.

The model's ability to reproduce tropical and extra tropical cyclone tracks was tested using the different tracking algorithms discussed in Methods. Figure 6 (a,b) shows cyclone track densities in the RegCM5 simulations and the ERA5 reanalysis calculated with the tracking algorithm of Reboita et al. (2010). The model has a good performance in locating the core of the trajectories in all regions but in some cases with differences in density from ERA5. While there is overestimation over the western Indian Ocean (coastal region of the Arabian Peninsula) and in the extratropical northern European areas, an underestimation occurs in western North America, southern Indian ocean and in the eastern coast of South America. The other two tropical cyclone tracking schemes (Figure 6d and 6e) also reproduce the areas of maximum track density but exhibit different behaviors in the western tropical Atlantic Ocean, southern Indian Ocean region, and eastern Asia tropical Pacific Ocean. The cyclone track density identified using the Reboita et al. (2010) and Fuentes-Franco et al. (2014, 2017) algorithms is underestimated in RegCM5 in the western tropical Atlantic compared to the Hodges (1994, 1995, 1999). However, the Hodges et al. (1994, 1995, 1999)'s algorithm overestimates track density in the eastern Asia tropical Pacific Ocean compared to the other two schemes. Differences are also found in the northern Australia coasts and southern Indian Ocean. These results highlight the importance of the choice of the tracking algorithm and the associated uncertainty in model results.

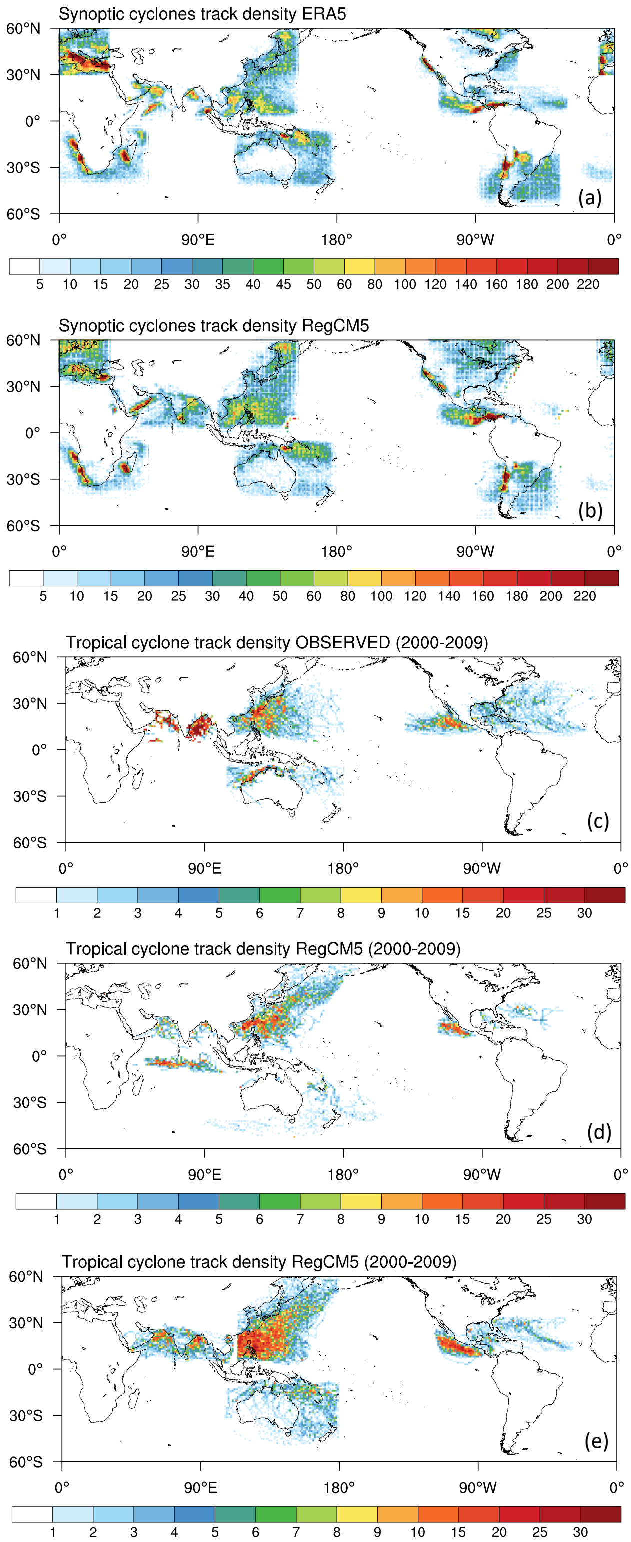

Figure 6. Total track density of all synoptic cyclones identified in ERA5 (panel a) and RegCM5 (panel b), from 2000 to 2009, using Reboita et al. (2010)'s algorithm. The unit is the number of cyclones with the center inside a 1° x 1° grid-box; total track density of tropical cyclones identified in the IBTrACS (panel c) and RegCM5 (panel d), from 2000 to 2009, using Fuentes-Franco et al. (2014, 2017)'s algorithm. The unit is the number of cyclones with the center inside a 1° x 1° grid-box; panel e is the same as panel d but using Hodges (1994, 1995, 1999)' algorithm.

Pan European CP domain

As mentioned, by being much more computationally efficient than previous versions of the model, RegCM5 allows simulations for a pan-European domain at convection-permitting resolution. Figure 7 illustrates a time sequence of summer convective events in the southern regions of Italy and Greece within the 3km CP domain, which is highlighted in the grey square, while ERA5 precipitation is shown outside of this region. The sequence starts on the night of June 8, 2000. A storm enters the CP domain from the western boundary, crossing Ireland throughout the day. Convection initiates in Sicily, Calabria, and northern Greece in the early afternoon, reaching its peak at 18:00 UTC and diminishing later in the evening. The time lapse demonstrates the consistency between the ERA5 boundary conditions and the CP model simulation in the evolution of the storm event.

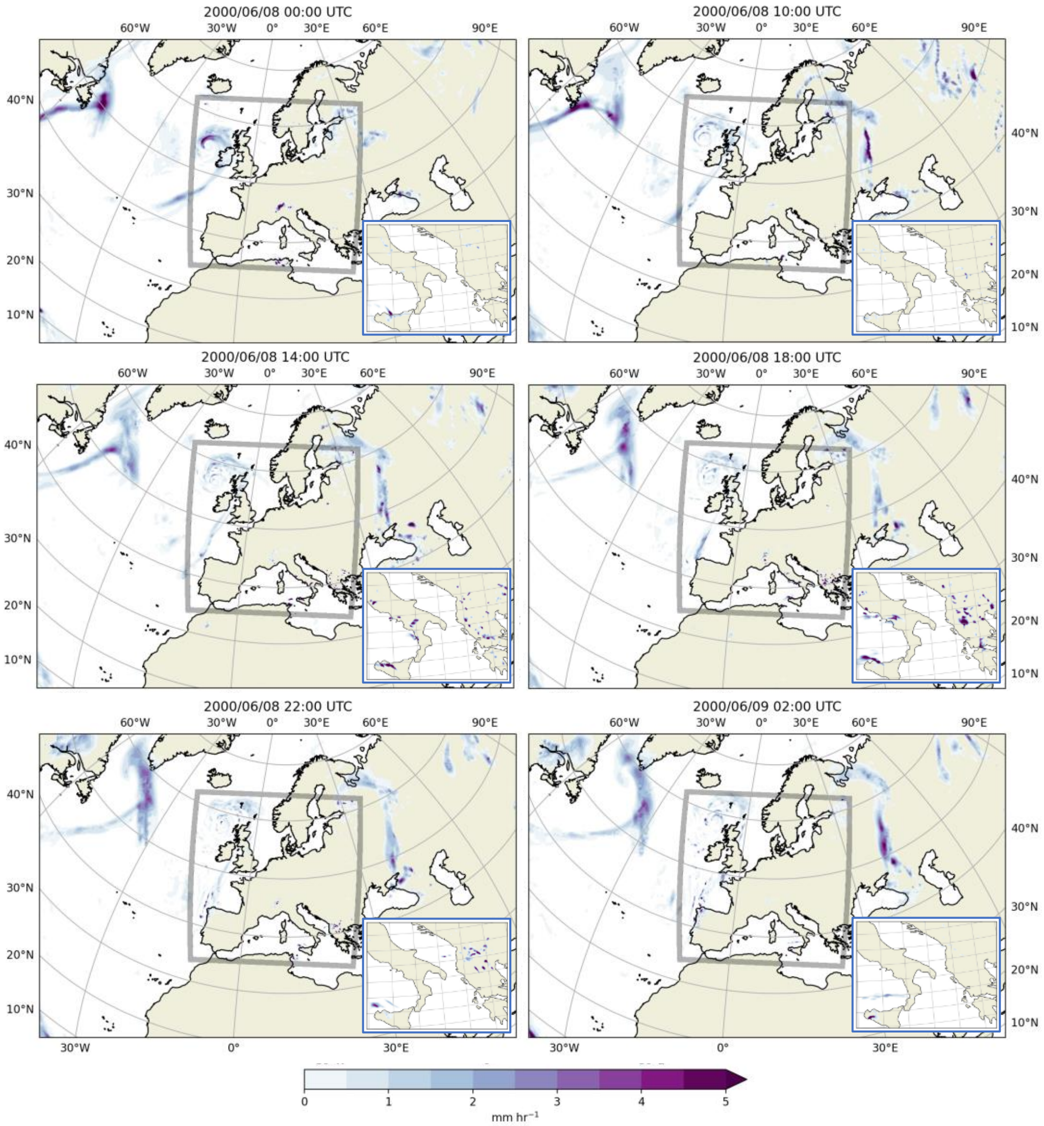

Figure 7. Precipitation estimates [mm hr^{-1}] from ERA5 and RegCM5 CP for 6 different time steps on the 8th and 9th June 2000. The precipitation estimates inside the gray box are from the RegCM5 CP simulation, while the rest of the domain outside the gray box shows the ERA5 precipitation estimates. The insert figure in each panel shows the REGCM5 CP precipitation estimates over a smaller section of the full domain to highlight the presence of the diurnal cycle in convective activity.

Figure 8 shows seasonal precipitation and temperature biases, precipitation frequency and intensity, and p99 biases for the convection-parametrized 12 km resolution run and the explicit convection 3km resolution run. Table 2 presents the observed datasets used for model validation, which are station-based or radar-based national datasets for various European countries. Both resolutions exhibit similar mean temperature and precipitation biases, mean daily bias frequency of events, while improvements in daily precipitation intensity and P99 biases at the 3km resolution are found, in particular reducing the dry bias in central northern Europe.

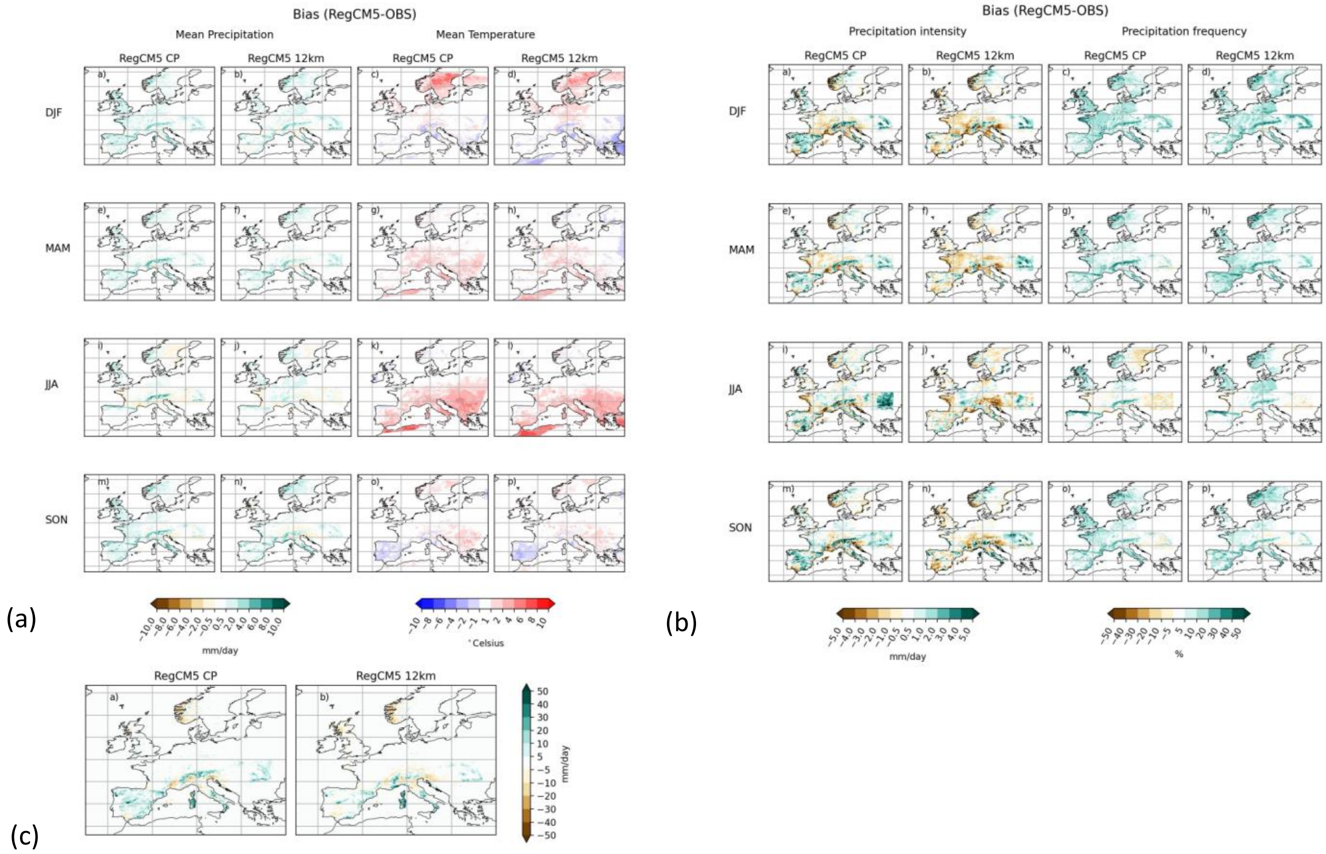

Figure 8. Mean seasonal bias for Europe CP and Europe 12 km simulation are shown as calculated with respect to the high resolution observation datasets. Mean seasonal daily precipitation and mean seasonal temperature are shown in panel a, the seasonal daily precipitation intensity and the precipitation frequency (> 1mm/day) in panel b and the annual P99 bias in panel c. For each variable the left column shows the CP simulation, while the right column represents the results for the Europe 12 km simulations.

Figure 9 compares precipitation probability density function distributions at a daily timescale for each observed dataset. The CP precipitation distribution aligns closely with the high-resolution datasets, outperforming the 12 km resolution model and ERA5 precipitation distribution in most regions. However, in Norway, the CP model distribution underestimates the observed one, and in the Carpathians and Spain regions, the model overestimates the precipitation distribution, possibly due to the lower resolution of station-based observations.

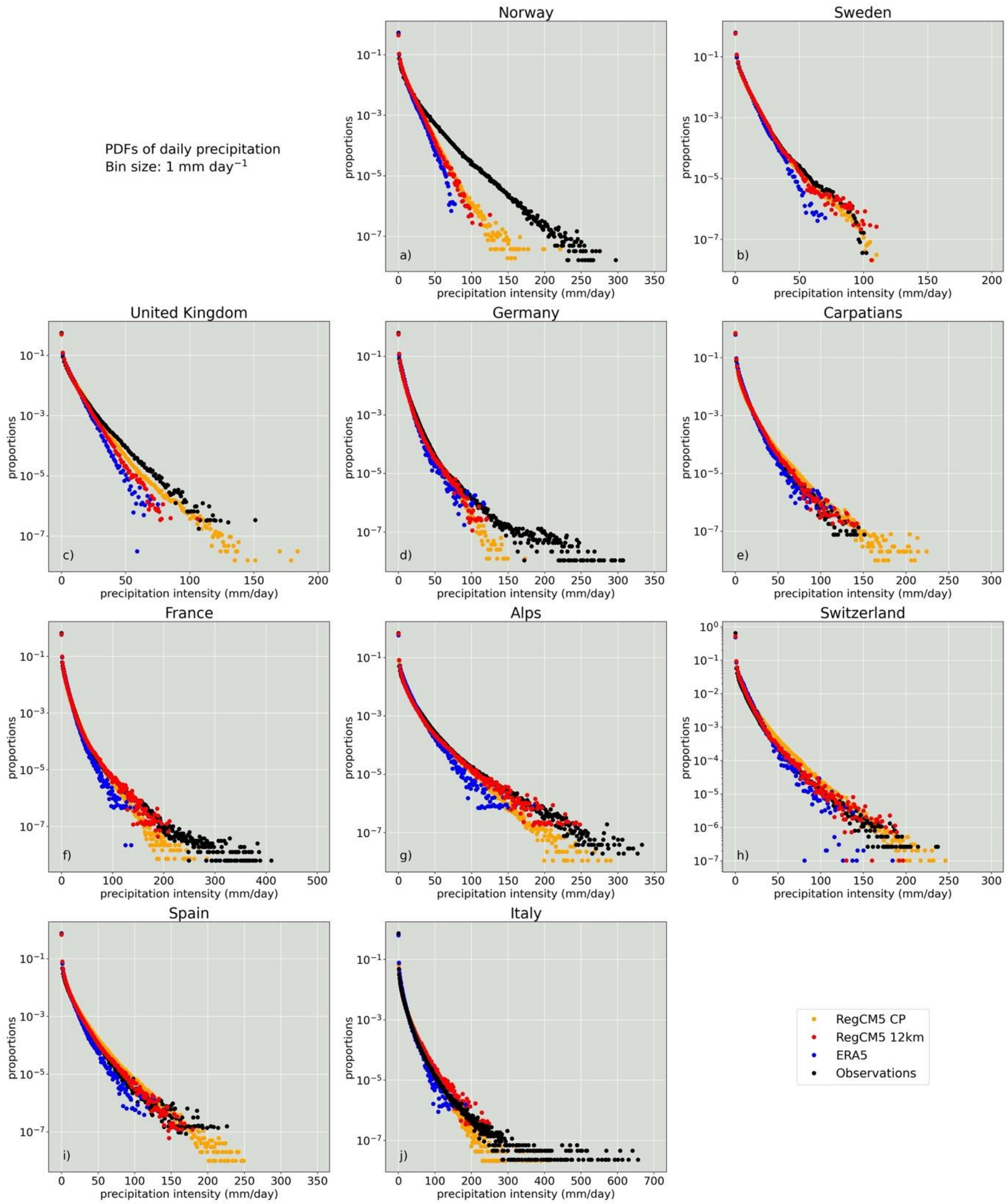

Figure 9. Probability density function distributions of the daily precipitation [mm day^{-1}] for the 10 regions investigated in the European domain. Each panel shows the distribution estimated from combining all available data in each domain for the years 2000-2004 for RegCM5 CP (orange), RegCM5 12km (red), ERA5 (blue) and observations (black). Details about the observational datasets for each region can be found in Table 2.

Supplementary Figure S8 illustrates daily temperature PDFs for the same regions, showing reasonable temperature distributions with a slight underestimation of maximum temperature values in areas of complex topography, such as the Alps and Swiss regions, likely attributed to a precipitation overestimation.

Finally, Figure 10, 11, and 12 present precipitation statistics at hourly timescale. Frequency, intensity, and very extreme hourly precipitation (p99.9) are computed for events above the threshold of 0.5 mm/h, revealing an orographically driven positive bias. Despite some regional discrepancies, the explicit representation of convection in the 3km resolution run improves systematic biases compared to the 12km simulation across all statistics and seasons. Supplementary Figures S9a-S9b show results with a more commonly used threshold of 0.1mm/h, indicating a noticeable negative and positive bias for intensity and frequency, respectively, in the 3km resolution, primarily attributed to very light events occurring between 0.1 and 0.5 mm/h. This is also evident in Figure 11, where the hourly precipitation distributions are reported for five regions. The high resolution model precipitation matches well the observed distribution with the only mismatch occurring in the range 0.1-0.5 mm/h for all the model resolutions and the ERA5 precipitation distributions.

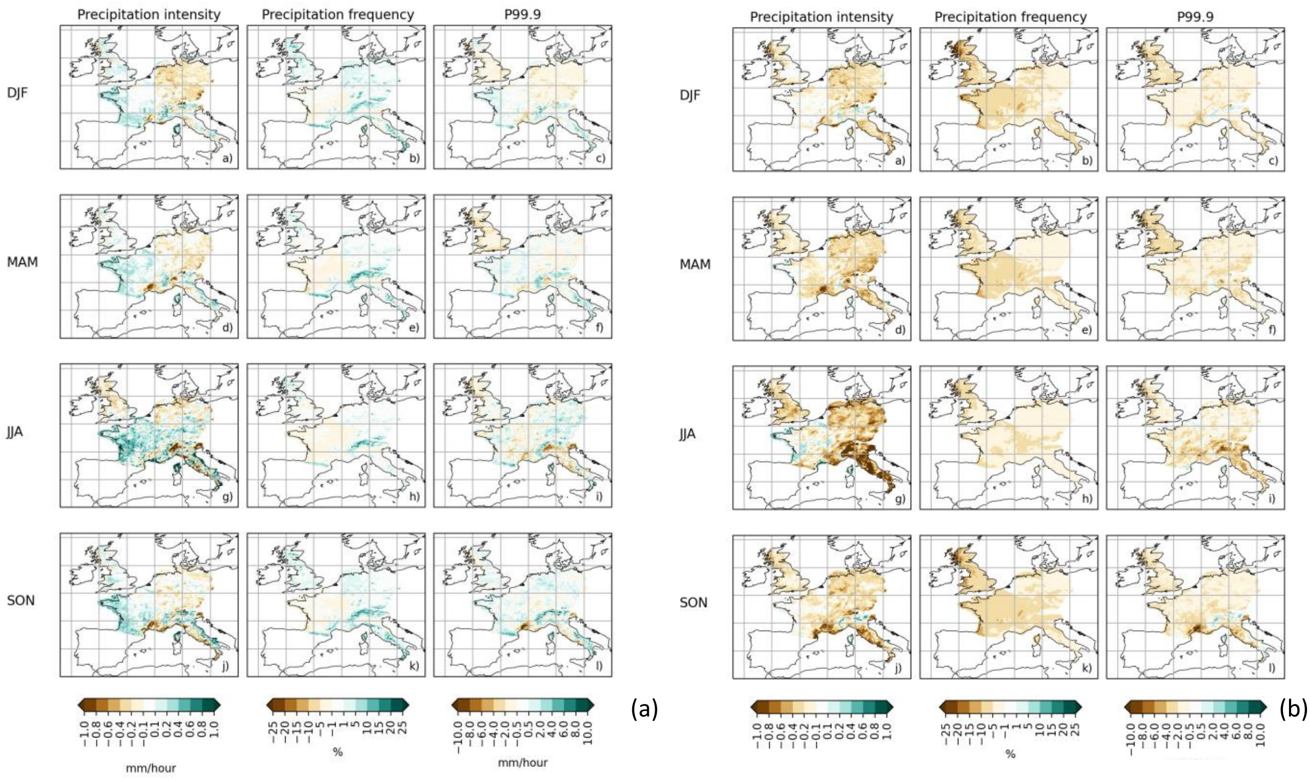

Figure 10: Precipitation intensity, wet frequency and P99.9 seasonal bias for hourly REGCM5 CP (panel a) and REGCM5 12km (panel b) versus high resolution observations. In each panel, the first column shows the seasonal biases for precipitation intensity, second column the precipitation frequency bias and the third column the P99.9 bias. The threshold used as the minimum precipitation for the REGCM5 simulations is 0.5 mm/hr. Figure S9 (panels a and b) shows the same seasonal biases but using the minimum threshold of 0.1 mm/hr.

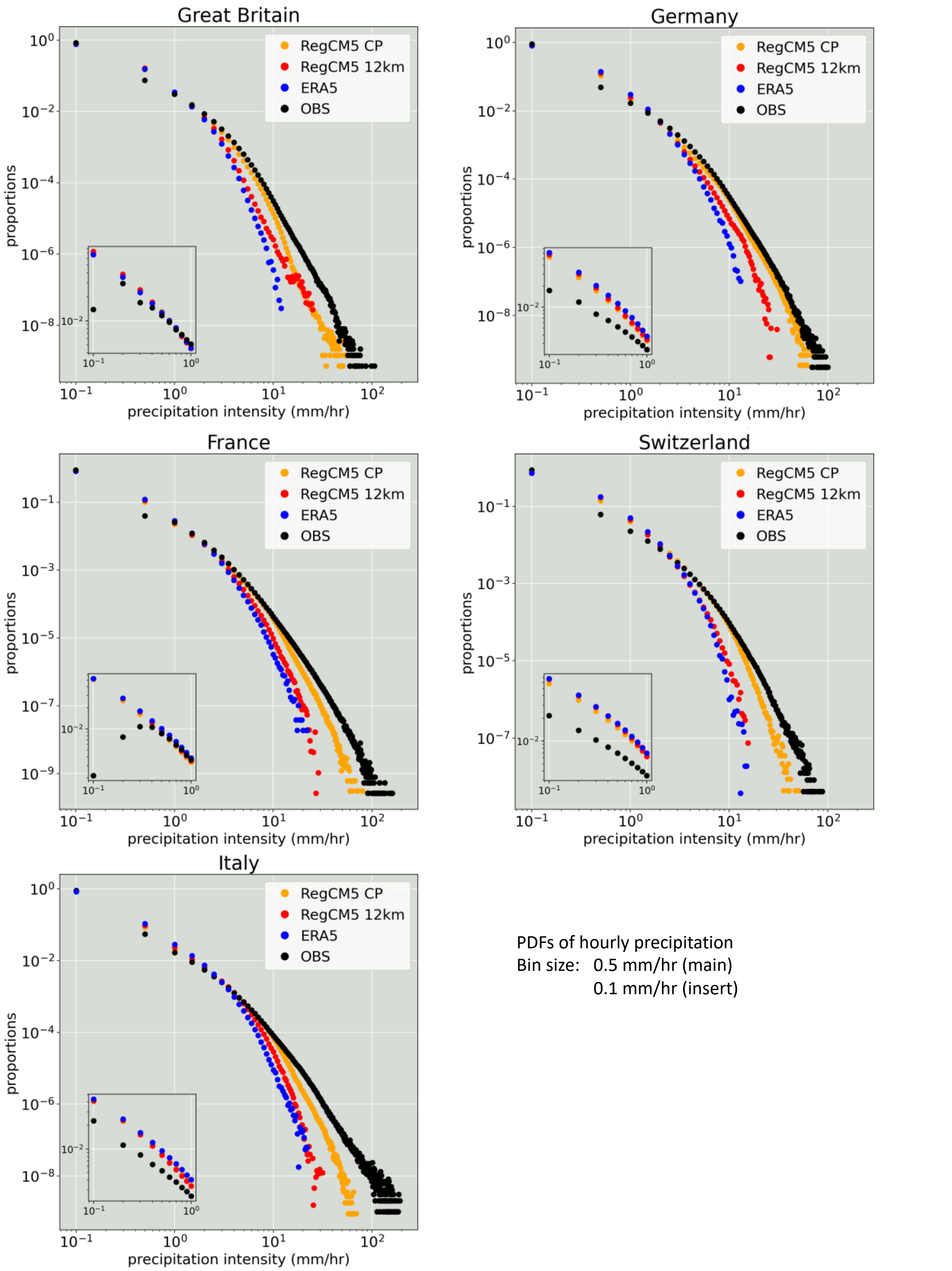

Figure 11. PDFs of hourly precipitation for the RegCM5 Convection Permitting simulation (orange), the RegCM5 12 km simulation (red), ERA5 (blue) and high resolution observations (black) from 5 regions (Great Britain, Germany, France, Switzerland and Italy). Each figure represents the distribution based on all the data available over the domain and time interval investigated. The bin size resolution is 0.5 mm/hr. The insert figure in each panel shows a breakdown of the three lowest precipitation intensity bins in the main panel, using a bin size resolution of 0.1 mm/hr.

Finally, Figure 12 shows the daily cycle of five precipitation statistics for the same five regions of Figure 11 and the JJA season. The explicit representation of convection successfully reproduces both the phase and amplitude of the diurnal cycle in most statistics and regions.The daily cycles for DJF, SON and MAM are reported in Figure S10 for completeness.

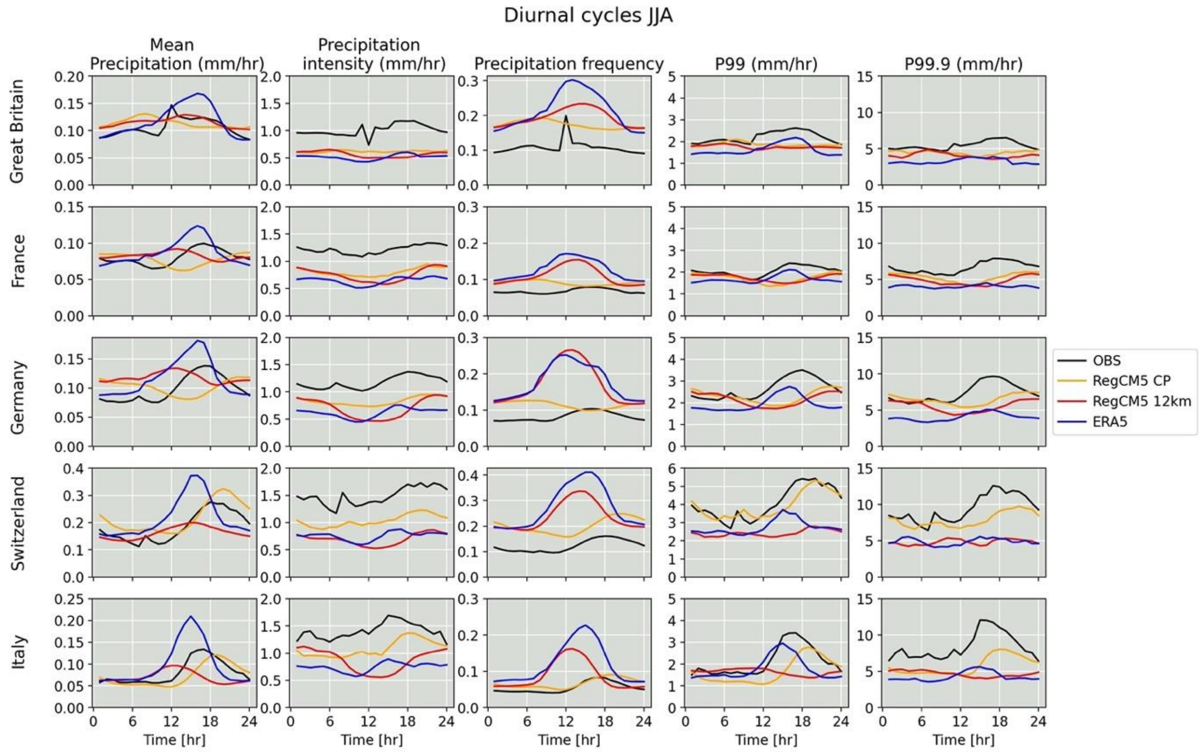

Figure 12: Diurnal cycles for mean precipitation (first column), precipitation intensity (second column), precipitation frequency (third column), p99 (fourth column) and p99.9 (fifth column) in JJA for 5 regions in Europe: Great Britain (top row), France (second row), Germany (third row), Switzerland (fourth row) and Italy (bottom row). The same figures for DJF, SON and MAM are shown in the Supplementary material.

Summary and Outlook

The Regional Climate Modeling system (RegCM) has evolved significantly since its inception, with versions such as RegCM4 and RegCM4-NH playing pivotal roles in climate research and participating in international projects such as CORDEX. These models, however, require relatively small time steps, and thus present limitations especially when applied at CP resolutions. The recently developed RegCM5 incorporates the dynamical core from the non-hydrostatic weather prediction model MOLOCH's to enhance model speed and stability. This paper aims to comprehensively evaluate the performance of RegCM5, focusing on convection-parametrized and convection-permitting scales across various CORDEX-CORE domains, and including for the first time a pan-European domain at convection-permitting resolution. The assessment encompasses temperature biases, precipitation patterns, monsoon circulations, extratropical and tropical cyclone tracks, and the model's ability to explicitly simulate convective events.

The evaluation of RegCM5 shows important improvements in addressing challenges posed by higher resolutions, offering improved capabilities for understanding climate dynamics and projections. The model demonstrates good performance in capturing temperature patterns, precipitation distributions, and monsoon circulations across various regions. The introduction of RegCM5's pan-European convection-permitting domain shows improved representation of daily and hourly precipitation distribution and diurnal cycle compared to the convection parametrized model version and illustrates the possibility to reach such resolution for larger model domains.

The model is currently available for use by the RegCM community and other prospective users. In this paper we have used for the different domains, model configurations that can be adopted as starting points for optimizing the model performance for different applications. Being a new development, the model needs to be further tested, and in this regard the contribution and feedback from the broader model community is essential. We are currently further improving the model capabilities, for example updating the land surface scheme CLM, the PBL scheme and including a two moment 6 hydrometeors microphysical scheme, and fine tuning some of the model's available physics options. We are also planning to develop a model version usable on GPU-based computing architectures. We expect that RegCM5 will be the basic model version used by the RegCM community and maintained by the ICTP development team over the next several years.

Data Availability Statement

The RegCM5 model code is available at the web site: https://zenodo.org/record/7548172#.Y8gVV7TMKUk.
The data used in this work can be found at the following web sites: http://www.euro4m.eu/datasets.html (EURO4M-APGD), https://cds.climate.copernicus.eu/cdsapp#!/dataset/reanalysis-era5-pressure-levels?tab=overview (ERA5).

References

Adler, R. F., Huffman, G. J., Chang, A., Ferraro, R., Xie, P., Janowiak, J., Rudolf, B., Schneider, U., Curtis, S., Bolvin, D., Gruber, A., Susskind, J., Arkin, P., & Nelkin, E. (2003). The version 2 global precipitation climatology project (GPCP) monthly precipitation analysis (1979–present). *Journal of Hydrometeorology*, *4*, 1147–1167. https://doi.org/10.1175/1525-7541(2003)004<1147:TVGPCP>2.0.CO;2.

Anthes RA, Hsie EY, Kuo YH (1987) Description of the Penn State/NCAR Mesoscale Model Version 4 (MM4). National Center for Atmospheric Research Tech Note TN-282+STR, NCAR, Boulder, CO

Artale V, Calmanti S, Carillo A, Dell'Aquila A and others (2010) An atmosphere–ocean regional climate model for the Mediterranean area: assessment of a present climate simulation. Clim Dyn 35: 721–740

Bae, J.; Sung, H.-J.; Baek, E.-H.; Choi, J.-H.; Lee, H.-J.; Kim, B.-M. (2023) Reduction in the Arctic Surface Warm Bias in the NCAR CAM6 by Reducing Excessive Low-Level Clouds in the Arctic. Atmosphere, 14, 522. https://doi.org/10.3390/atmos14030522

Ban, N., Caillaud, C., Coppola, E., Pichelli, E., Sobolowski, S., Adinolfi, M., et al. (2021). The first multi-model ensemble of regional climate simulations at kilometer-scale resolution part 1: Evaluation of precipitation. Climate Dynamics, 57(1–2), 275–302. https://doi.org/10.1007/s00382-021-05708-w

Beck, H. E., Pan, M., Roy, T., Weedon, G. P., Pappenberger, F., van Dijk, A. I. J. M., Huffman, G. J., Adler, R. F., and Wood, E. F.: Daily evaluation of 26 precipitation datasets using Stage-IV gauge-radar data for the CONUS, Hydrol. Earth Syst. Sci., 23, 207–224, https://doi.org/10.5194/hess-23-207-2019, 2019.

Bettolli, M., Solman, S., da Rocha, R. et al (2021) The CORDEX flagship pilot study in southeastern South America: a comparative study of statistical and dynamical downscaling models in simulating daily extreme precipitation events. Clim Dyn 56(5):1589–1608

Bretherton CS, McCaa JR, Grenier H (2004) A new parameterization for shallow cumulus convection and its application to marine subtropical cloud-topped boundary layers. I. Description and 1D results. Mon Weather Rev 132:864–882

Buzzi, A., Davolio, S., malguzzi, P., Drofa, O., & Mastrangelo, D. (2014). Heavy rain episodes over Liguria in autumn 2011: Numerical forecast- ing experiments. Natural Hazards and Earth System Sciences, 14(5), 1325–1340. https://doi.org/10.5194/nhess-14-1325-2014

Chen, M., Shi, W., Xie, P., Silva, V. B. S., Kousky, V. E., Higgins, R. W., and Janowiak, J. E.: Assessing objective techniques for gauge-based analyses of global daily precipitation, J. Geophys. Res.-Atmos., 113, D04110, https://doi.org/10.1029/2007jd009132, 2008.

Coppola E, Giorgi F, Mariotti L, Bi X (2012) RegT-Band: a tropical band version of RegCM4. Clim Res 52:115-133. https://doi.org/10.3354/cr01078

Coppola, E., Sobolowski, S., Pichelli, E. et al. A first-of-its-kind multi-model convection permitting ensemble for investigating convective phenomena over Europe and the Mediterranean. Clim Dyn 55, 3–34 (2020). https://doi.org/10.1007/s00382-018-4521-8

Coppola, E., Stocchi, P., Pichelli, E., Torres Alavez, J. A., Glazer, R., Giuliani, G., Di Sante, F., Nogherotto, R., and Giorgi, F.: Non-Hydrostatic RegCM4 (RegCM4-NH): model description and case studies over multiple domains, Geosci. Model Dev., 14, 7705–7723, https://doi.org/10.5194/gmd-14-7705-2021, 2021.

Cornes R, van der Schrier G, van den Besselaar EJM, Jones PD (2018) An ensemble version of the E-OBS temperature and precipitation datasets. J Geophys Res Atmos. https://doi. org/10.1029/2017JD028200

Cressman, G. P. (1959). An operational objective analysis system. *Monthly Weather Review*, *87*(10), 367-374.

da Rocha, R. P., Llopart, M., Reboita, M. S., Bettolli, M. L., Solman, S., Fernádez, J., Milovac, J., Feijoó, M.; Coppola, E. (2023). Precipitation diurnal cycle assessment in convection-permitting simulations in Southeastern South America. Accepted to publication at Earth Systems and Environment.

Davolio S., P. Malguzzi, O. Drofa, D. Mastrangelo and A. Buzzi (2020): The Piedmont flood of November 1994: a test-bed of forecasting capabilities of the CNR-ISAC meteorological model suite. Bull. of Atmos. Sci. & Technol.

Dickinson, R.E., Errico, R.M., Giorgi, F., Bates, G.T. (1989) A regional climate model for the western United States. *Climatic Change*, 15 (3), pp. 383-422. doi: 10.1007/BF00240465

Dickinson, R. E., Henderson-Sellers, A., & Kennedy, P. J. (1993). *Biosphere-atmosphere Transfer Scheme (BATS) Version 1e as Coupled to the NCAR Community Climate Model* (No. NCAR/TN-387+STR). University Corporation for Atmospheric Research. doi:10.5065/D67W6959

Di Sante, F., Coppola, E., Farneti, R., & Giorgi, F. (2019). Indian Summer Monsoon as simulated by the regional earth system model RegCM-ES: the role of local air–sea interaction. Climate Dynamics, 1-20.

Emanuel KA, Zivkovic-Rothman M (1999) Development and evaluation of a convection scheme for use in climate models. J Atmos Sci 56: 1766–1782

Fairall, C.W., E. F. Bradley, J. E. Hare, A. A. Grachev, and J. B. Edson, 2003: Bulk Parameterization of Air-Sea Fluxes: Updates and Verification for the COARE Algorithm. J. Climate, 16, pp 571-591.

Fantini, A.: Climate change impact on flood hazard over Italy, Ph.D. thesis, University of Trieste, 2019.

Fuentes-Franco, R., Coppola, E., Giorgi, F. *et al.* (2014) Assessment of RegCM4 simulated inter-annual variability and daily-scale statistics of temperature and precipitation over Mexico. *Clim Dyn* **42**, 629–647 . https://doi.org/10.1007/s00382-013-1686-z

Fuentes-Franco, R., Giorgi, F., Coppola, E. et al. (2017) Sensitivity of tropical cyclones to resolution, convection scheme and ocean flux parameterization over Eastern Tropical Pacific and Tropical North Atlantic Oceans in the RegCM4 model. *Clim Dyn* 49, 547–561 . https://doi.org/10.1007/s00382-016-3357-3

Gao, X.J. & Giorgi, F. (2017) Use of the RegCM system over East Asia: review and perspectives. Engineering, 3(5), 766–772.

Gelaro, Ronald, McCarty, Will, Suarez, Max J., Todling, Ricardo, Molod, Andrea, Takacs, Lawrence, Randles, Cynthia A., Darmenov, Anton, Bosilovich, Michael G., Reichle, Rolf, Wargan, Krzysztof, Coy, Lawrence, Cullather, Richard, Draper, Clara, Akella, Santha, Buchard, Virginie, Conaty, Austin, da Silva, Arlindo M., Gu, Wei, Kim, Gi-Kong, Koster, Randal, Lucchesi, Robert, Merkova, Dagmar, Nielsen, Jon Eric, Partyka, Gary, Pawson, Steven, Putman, William, Rienecker, Michele, Schubert, Siegfried D., Sienkiewicz, Meta, Zhao, Bin. (2017) The Modern-Era Retrospective Analysis for Research and Applications, Version 2 (MERRA-2). J. Clim.. Vol. 30, No. 14, pp. 5419-5454. DOI: 10.1175/JCLI-D-16-0758.1 ISSN: 0894-8755

Giorgi, F., Bates, G. T. (1989). The climatological skill of a regional model over complex terrain. Monthly Weather Review, 117 (11), pp. 2325-2347.

Giorgi, F., Marinucci, M. R., & Bates, G. T. (1993). Development of a second generation regional climate model (RegCM2). Part I: Boundary layer and radiative transfer processes. Monthly Weather Review, 121(10), 2794–2813.

Giorgi, F., & Mearns, L. O. (1999). Introduction to special section: Regional climate modeling revisited. Journal of Geophysical Research, 104(D6), 6335–6352. https://doi.org/10.1029/98jd02072

Giorgi F, Francisco R, Pal JS (2003) Effects of a sub-grid scale topography and landuse scheme on surface climate and hydrology. I. Effects of temperature and water vapor disaggregation. J Hydrometeorol 4: 317–333

Giorgi, F., Jones, C., & Asrar, G. (2009). Addressing climate information needs at the regional level: The CORDEX framework. World Meteor- ological Organization Bulletin, 58, 175–183.

Giorgi, F., Coppola, E., Solmon, F., Mariotti, L., Sylla, M., Bi, X., et al. (2012). RegCM4: Model description and preliminary tests over multiple CORDEX domains. Climate Research, 52, 31–48. https://doi.org/10.3354/cr01018

Giorgi, F., Coppola, E., Jacob, D., ..., Pichelli, E., et al. (2021). The CORDEX- CORE EXP-I initiative: Description and highlight results from the initial analysis, Bulletin of the American Meteorological Society (published online ahead of print 2021). https://journals.ametsoc.org/view/journals/bams/aop/BAMS-D-21- 0119.1/BAMS-D-21-0119.1.xml

Giorgi, F., Coppola, E., Giuliani, G., Ciarlò, J.M., Pichelli, E., Nogherotto, R., Raffaele, F., Malguzzi, P., Davolio, S., Stocchi, P., Drofa, O. (2023) The fifth generation regional climate modeling system, RegCM5. Part I: Description and illustrative examples at parameterized convection and convection-permitting resolutions. *Journal of Geophysical Research: Atmospheres*. DOI:10.1029/2022JD038199

Glazer H. R., E. Coppola, F. Giorgi, Understanding Nocturnally-driven Extreme Precipitation Events over Lake Victoria in a Convection-Permitting Model, Monthly Weather Review, accepted (2023)

Grell, G. A., 1993: Prognostic Evaluation of Assumptions Used by Cumulus Parameterizations. *Mon. Wea. Rev.*, **121**, 764–787, https://doi.org/10.1175/1520-0493(1993)121<0764:PEOAUB>2.0.CO;2.

Grell, G., Dudhia, J., & Stauffer, D. R. (1994). A description of the fifth generation Penn State/NCAR Mesoscale Model (MM5) (p. 121). NCAR technical note NCAR/TN-398 + STR.

Güttler, I., Branković, Č., O'Brien, T.A. *et al.* Sensitivity of the regional climate model RegCM4.2 to planetary boundary layer parameterisation. *Clim Dyn* **43**, 1753–1772 (2014). https://doi.org/10.1007/s00382-013-2003-6

Gutowski, W. J., Giorgi, F., Timbal, B., Frigon, A., Jacob, D., Kang, H.-S., et al. (2016). WCRP coordinated regional downscaling EXperiment (CORDEX): A diagnostic MIP to CMIP6. Geoscientific Model Development, 9, 4087–4095.\

Harris, I., Osborn, T.J., Jones, P. *et al.* Version 4 of the CRU TS monthly high-resolution gridded multivariate climate dataset. *Sci Data* **7**, 109 (2020). https://doi.org/10.1038/s41597-020-0453-3

Hart, R. E. (2003). A cyclone phase space derived from thermal wind and thermal asymmetry. *Monthly weather review*, *131*(4), 585-616.

Herrera, S., Gutiérrez, J. M., Ancell, R., Pons, M. R., Frías, M. D., & Fernández, J. (2012). Development and analysis of a 50-year high-resolution daily gridded precipitation dataset over Spain (Spain02). *International Journal of Climatology*, *32*(1), 74-85.

Hersbach, H. *et al.* The ERA5 global reanalysis. *Q. J. R. Meteorol. Soc.* 146, 1999–2049 (2020). https://doi.org/10.1002/qj.3803

Hodges, K.I. (1994) A general-method for tracking analysis and its application to meteorological data. Mon Weather Rev 122(11):2573–2586. https://doi.org/10.1175/1520-0493(1994)122<2573:AGMFT A>2.0.CO;2

Hodges, K.I. (1995) Feature tracking on the unit sphere. Mon Weather. Rev 123(12):3458–3465. https ://doi.org/10.1175/1520-0493(1995)123<3458:FTOTU S>2.0.CO;2

Hodges, K.I. (1999) Adaptive constraints for feature tracking. Mon. Weather. Rev., 127, 1362–1373. https://doi.org/10.1175/1520-0493(1999)127<1362:ACFFT>2.0.CO;2

Hodges, K., Cobb, A., & Vidale, P. L. (2017). How well are tropical cyclones represented in reanalysis datasets?. *Journal of Climate*, *30*(14), 5243-5264.

Hoffmann, P., Reinhart, V., Rechid, D., de Noblet-Ducoudré, N., Davin, E. L., Asmus, C., Bechtel, B., Böhner, J., Katragkou, E., and Luyssaert, S.(2023) High-resolution land use and land cover dataset for regional climate modelling: historical and future changes in Europe, Earth Syst. Sci. Data, 15, 3819–3852, https://doi.org/10.5194/essd-15-3819-2023.

Holtslag A, de Bruijn E, Pan HL (1990) A high resolution air mass transformation model for short-range weather forecasting. Mon Weather Rev 118: 1561–1575

Hong, S.-Y., Dudhia, J. and Chen, S.-H. (2004) A Revised Approach to Ice Microphysical Processes for the Bulk Parameterization of Clouds and Precipitation. Monthly Weather Review, 132, 103-120

Hoskins, Brian John and Hodges, Kevin Ivan (2002) *New perspectives on the Northern Hemisphere winter storm tracks.* Journal of the Atmospheric Sciences, 59 (6). pp. 1041-1061. ISSN1520-0469 doi: https://doi.org/10.1175/1520-0469(2002)059<1041:NPOTNH>2.0.CO;2

Hostetler SW, Bates GT, Giorgi F (1993) Interactive nesting of a lake thermal model within a regional climate model for climate change studies. J Geophys Res 98: 5045–5057

Isotta, F., Frei, C., Weilguni, V., Perčec Tadić, M., Lassegues, P., Rudolf, B., Pavan, V., Cacciamani, C., Antolini, G., Ratto, S., Munari, M., Micheletti, S., Bonati, V., Lussan, C., Ronchi, C., Panettieri, E., Marigo, G., Vertačnik, G. (2014). The climate of daily precipitation in the Alps: Development and analysis of a high-resolution grid dataset from pan-Alpine rain-gauge data. International Journal of Climatology. DOI:10.1002/joc.3794

Iturbide M, Gutiérrez JM, Alves L, Bedia J, Cerezo-Mota R, Di Luca A, Faria SH, Gorodetskaya I, Hauser M, Herrera S, Hennessy KJ, Jones R, Krakovska S, Manzanas R, Martínez-Castro D, Narisma GT, Pinto I, Seneviratne SI, van den Hurk B, Vera CS (2020) An update of IPCC physical climate reference regions for subcontinental analysis of climate model data: Definition and aggregated datasets. Earth Syst Sci Data. https://doi.org/10.5194/essd-12-2959-2020

Johansson, B. (2000) Areal Precipitation and Temperature in the Swedish Mountains. An evaluation from a hydrological perspective. Nordic Hydrology, 31, 207-228.

Kain, J. S. (2004). The Kain–Fritsch Convective Parameterization: An Update, Journal of Applied Meteorology, 43(1), 170-181

Kiehl J, Hack J, Bonan G, Boville B, Breigleb B, Williamson D, Rasch P (1996) Description of the NCAR Community Climate Model (CCM3). National Center for Atmospheric Research Tech Note NCAR/TN-420+ STR, NCAR, Boulder, CO

Knapp KR, Kruk MC, Levinson DH, Diamond HJ, Neumann CJ (2010) The International Best Track Archive for Climate Stewardship (IBTrACS): unifying tropical cyclone best track data. Bull Am Meteor Soc 91:363–376. https://doi.org/10.1175/2009BAMS27 55.1

Knapp KR, Diamond HJ, Kossin JP, Kruk MC, Schreck CJ (2018) International Best Track Archive for Climate Stewardship (IBTrACS) Project, Version 4. NOAA National Centers for Environmental Information. https://doi.org/10.25921/82ty-9e16. Accessed 10/09/2019

Kreklow, J.; Tetzlaff, B.; Burkhard, B.; Kuhnt, G. Radar-Based Precipitation Climatology in Germany-Developments, Uncertainties and Potentials. *Atmosphere* **2020**, *11*, 217. https://doi.org/10.3390/atmos11020217

Kummerow, C., and Coauthors, 2000: The Status of the Tropical Rainfall Measuring Mission (TRMM) after Two Years in Orbit. *J. Appl. Meteor. Climatol.*, **39**, 1965–1982, https://doi.org/10.1175/1520-0450(2001)040<1965:TSOTTR>2.0.CO;2.

Lewis E, Quinn N, Blenkinsop S, Fowler HJ, Freer J, Tanguy M, Hitt O, Coxon G, Bates P, Woods R, Fry M, Chevuturi A, Swain O, White SM (2022). Gridded estimates of hourly areal rainfall for Great Britain 1990-2016 [CEH-GEAR1hr] v2. NERC EDS Environmental Information Data Centre. (Dataset). https://doi.org/10.5285/fc9423d6-3d54-467f-bb2b-fc7357a3941f

Liang, X.-Z. and Wu, X.(2005) Evaluation of a GCM subgrid cloud-radiation interaction parameterization using cloud-resolving model simulations, Geophys. Res. Lett., 32, L06801, https://doi.org/10.1029/2004GL022301.

Lipzig, N.P.M.v., Walle, J.V.d., Belušić, D. et al. Representation of precipitation and top-of-atmosphere radiation in a multi-model convection-permitting ensemble for the Lake Victoria Basin (East-Africa). Clim Dyn 60, 4033–4054 (2023). https://doi.org/10.1007/s00382-022-06541-5

Liu, L., Solmon, F., Vautard, R., Hamaoui-Laguel, L., Torma, C. Z., and Giorgi, F.(2016): Ragweed pollen production and dispersion modelling within a regional climate system, calibration and application over Europe, Biogeosciences, 13, 2769–2786

Malguzzi, P., Grossi, G., Buzzi, A., Ranzi, R., & Buizza, R. (2006). The 1966 "century" flood in Italy: A meteorological and hydrological revisitation. *Journal of Geophysical Research*, *101*(D24), D24106. https://doi.org/10.1029/2006jd007111

Mlawer, E.J., S.J. Taubman, P.D. Brown, M.J. Iacono and S.A. Clough (1997a) RRTM, a validated correlated-k model for the longwave. J. Geophys. Res., 102, 16,663-16,682

Mlawer, E.J., and S.A. Clough, On the extension of rapid radiative transfer model to the shortwave region (1997b), in Proceedings of the 6th Atmospheric Radiation Measurement (ARM) Science Team Meeting, U.S. Department of Energy, CONF-9603149

Mohr, M. (2009). Comparison of versions 1.1 and 1.0 of gridded temperature and precipitation data for Norway. *Norwegian Meteorological Institute, met no note*, *19*, 475.

Nogherotto, R., Tompkins, A. M., Giuliani, G., Coppola, E., and Giorgi, F. (2016) Numerical framework and performance of the new multiple-phase cloud microphysics scheme in RegCM4.5: precipitation, cloud microphysics, and cloud radiative effects, Geosci. Model Dev., 9, 2533–2547

Oleson, K.W., D.M. Lawrence, G.B. Bonan, B. Drewniak, M. Huang, C.D. Koven, S. Levis, F. Li, W.J. Riley, Z.M. Subin, S.C. Swenson, P.E. Thornton, A. Bozbiyik, R. Fisher, E. Kluzek, J.-F. Lamarque, P.J. Lawrence, L.R. Leung, W. Lipscomb, S. Muszala, D.M. Ricciuto, W. Sacks, Y. Sun, J. Tang, Z.-L. Yang, 2013: Technical Description of version 4.5 of the Community Land Model (CLM). Ncar Technical Note NCAR/TN-503+STR, National Center for Atmospheric Research, Boulder, CO, 422 pp

Pal, J. S., Small, E. E., and Eltahir, E. A. B.: Simulation of regional-scale water and energy budgets: Representation of subgrid cloud and precipitation processes within RegCM, J. Geophys. Res., 105, 29579–29594, 2000

Pal, J. S., & Coauthors (2007). The ICTP RegCM3 and RegCNET: Regional climate modeling for the developing World. *Bulletin American Meteorology Social*, *88*, 1395–1409.

Pichelli, E., Coppola, E., Sobolowski, S., Ban, N., Giorgi, F., Stocchi, P., et al. (2021). The first multi-model ensemble of regional climate simulations at kilometer-scale resolution part 2: Historical and future simulations of precipitation. *Climate Dynamics*, *56*(11–12), 3581–3602. https:// doi.org/10.1007/s00382-021-05657-4

Ratnam, J.V., Giorgi, F., Kaginalkar, A. et al. (2009) Simulation of the Indian monsoon using the RegCM3–ROMS regional coupled model. Clim Dyn 33, 119–139

Rauthe, M., Steiner, H., Riediger, U., Mazurkiewicz, A., & Gratzki, A. (2013). A Central European precipitation climatology–Part I: Generation and validation of a high-resolution gridded daily data set (HYRAS). *Meteorologische Zeitschrift*, *22*(3), 235-256.

Reale, M., Giorgi, F., Solidoro, C., Di Biagio, V., Di Sante, F., & Mariotti, L., et al. (2020). The regional Earth system Model RegCM-ES: Evaluation of the Mediterranean climate and marine biogeochemistry. Journal of Advances in Modeling Earth Systems, 12, e2019MS001812

Reboita, M. S., da Rocha, R. P., Ambrizzi, T., & Sugahara, S. (2010). South Atlantic Ocean cyclogenesis climatology simulated by regional climate model (RegCM3). Climate Dynamics, 35(7–8), 1331–1347. https://doi.org/10.1007/s00382-009-0668-7

Shalaby, A., Zakey, A. S., Tawfik, A. B., Solmon, F., Giorgi, F., Stordal, F., Sillman, S., Zaveri, R. A., and Steiner, A. L (2012). Implementation and evaluation of online gas-phase chemistry within a regional climate model (RegCM-CHEM4), Geosci. Model Dev., 5, 741–760

Shi, Y., Yu, M., Erfanian, A., & Wang, G. (2018). Modeling the Dynamic Vegetation–Climate System over China Using a Coupled Regional Model, Journal of Climate, 31(15), 6027-6049

Sitz, L. E., di Sante, F., Fantini, R., Fuentes-Franco, R., Coppola, E., Mariotti, L., et al. (2017). Description and evaluation of the Earth System Regional Climate model (RegCM-ES). Journal of Advances in Modeling Earth Systems, 9(4), 1863–1886. https://doi.org/10.1002/2017ms000933

Solmon F, Giorgi F, Liousse C (2006) Aerosol modeling for regional climate studies: application to anthropogenic particles and evaluation over a European/African domain. Tellus Ser B Chem Phys Meterol 58: 51–72

Solmon F, Mallet M, Elguindi N, Giorgi F, Zakey A, Konaré A (2008) Dust aerosol impact on regional precipitation over western Africa, mechanisms and sensitivity to absorption properties. Geophys Res Lett 35: L24705, doi: 10.1029/2008GL035900

Steiner AL, Pal JS, Rauscher SA, Bell JL and others (2009) Land surface coupling in regional climate simulations of the West Africa monsoon. Clim Dyn 33: 869–892

Sundqvist, H., (1988): Parametrization of condensation and associated clouds in models for weather prediction and general circulation simulation. Physically-Based Modelling and Simulation of Climate and Climate Change, M. E. Schlesinger, Ed., Kluwer, 433–461

Szalai, S., Auer, I., Hiebl, J., Milkovich, J., Radim, T., Stepanek, P., Zahradnicek, P., Bihari, Z., Lakatos, M., Szentimrey, T., Limanowka, D., Kilar, P., Cheval, S., Deak, Gy., Mihic, D., Antolovic, I., Mihajlovic, V., Nejedlik, P., Stastny, P., Mikulova, K., Nabyvanets, I., Skyryk, O., Krakovskaya, S., Vogt, J., Antofie, T. and Spinoni, J. 2013. Climate of the Greater Carpathian Region. Final Technical Report. Available at www.carpatclim-eu.org/pages/download/

Tabary, P., Dupuy, P., L'henaff, G., Gueguen, C., Moulin, L., Laurantin, O., Merlier, C., and Soubeyroux, J.M., 2012. A 10-year (1997–2006) reanalysis of Quantitative Precipitation Estimation over France: methodology and first results. Weather Radar and Hydrology, IAHS Publ. 351, 255-260.

Teichmann, C., Jacob, D., Remedio, A.R. *et al.* Assessing mean climate change signals in the global CORDEX-CORE ensemble. *Clim Dyn* **57**, 1269–1292 (2021). https://doi.org/10.1007/s00382-020-05494-x

Tiedtke M (1989) A comprehensive mass-flux scheme for cumulus parameterization in large-scale models. Mon Weather Rev 117: 1779–1800

Trini Castelli, S., Bisignano, A., Donateo, A., Landi, T. C., Martano, P., & Malguzzi, P. (2020). Evaluation of the turbulence parameterization in the MOLOCH meteorological model. Quarterly Journal of the Royal Meteorological Society, 146, 124–141.

Turuncoglu, U.U., Sannino, G. (2017) Validation of newly designed regional earth system model (RegESM) for Mediterranean Basin. Clim Dyn 48, 2919–2947

Wu, J., & GAO, X. J. (2013). A gridded daily observation dataset over China region and comparison with the other datasets. *Chinese Journal of Geophysics*, *56*(4), 1102-1111.

Wüest, M., C. Frei, A. Altenhoff, M. Hagen, M. Litschi, and C. Schär (2010). A gridded hourly precipitation dataset for Switzerland using rain-gauge analysis and radar-based disaggregation. International Journal of Climatology 30(12), 1764–1775.

Xu, K.-M., and D. A. Randall, 1996: A semiempirical cloudiness parameterization for use in climate models. J. Atmos. Sci., 53, 3084-3102.

Xu Y, Gao XJ, Yan SY, Xu CH, Shi Y, Giorgi F (2009) A daily temperature dataset over China and its application in validating a RCM simulation. Adv Atmos Sci 26:763–772

Yatagai, A., O. Arakawa, K. Kamiguchi, H. Kawamoto, M. I. Nodzu, and A. Hamada, 2009: A 44-year daily gridded precipitation dataset for Asia based on a dense network of rain gauges. *SOLA*, **5**, 137–140, doi:10.2151/sola.2009-035.

Zakey AS, Solmon F, Giorgi F (2006) Implementation and testing of a desert dust module in a regional climate model. Atmos Chem Phys 6: 4687–4704

Zakey AS, Giorgi F, Bi X (2008) Modeling of sea salt in a regional climate model: fluxes and radiative forcing. J Geophys Res 113: D14221, doi:10.1029/2007JD009209

Zeng X, Zhao M, Dickinson RE (1998) Intercomparison of bulk aerodynamic algorithms for the computation of sea surface fluxes using TOGA COARE and TAO data. J Clim 11: 2628–2644

Zeng X, Beljaars A (2005) A prognostic scheme of sea surface skin temperature for modeling and data assimilation. Geophys Res Lett 32: L14605, doi:10.1029/ 2005 GL023030

Supplementary Figures.

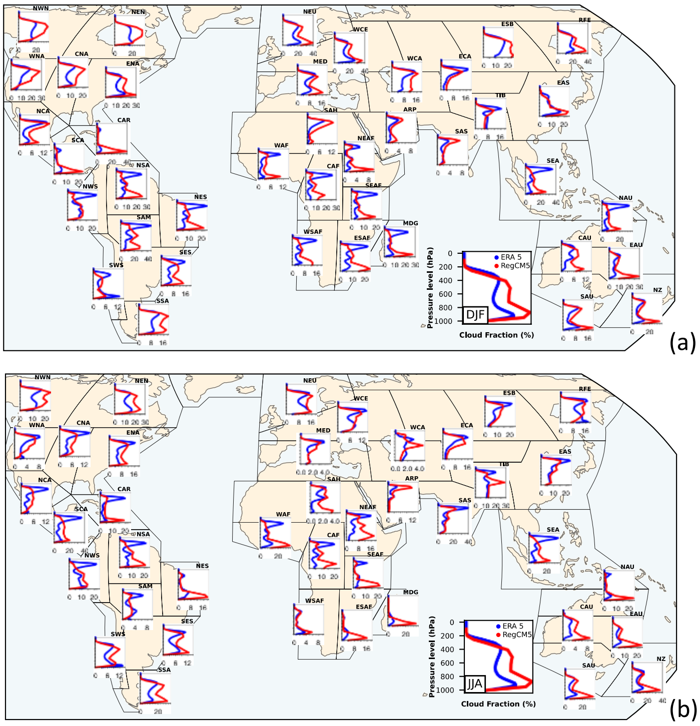

Figure S1: Cloud fraction vertical profiles for DJF (a) and JJA (b). The period covered is 2000-2009, except for the European domain (MED, WCE and NEU regions): 1980-2010.

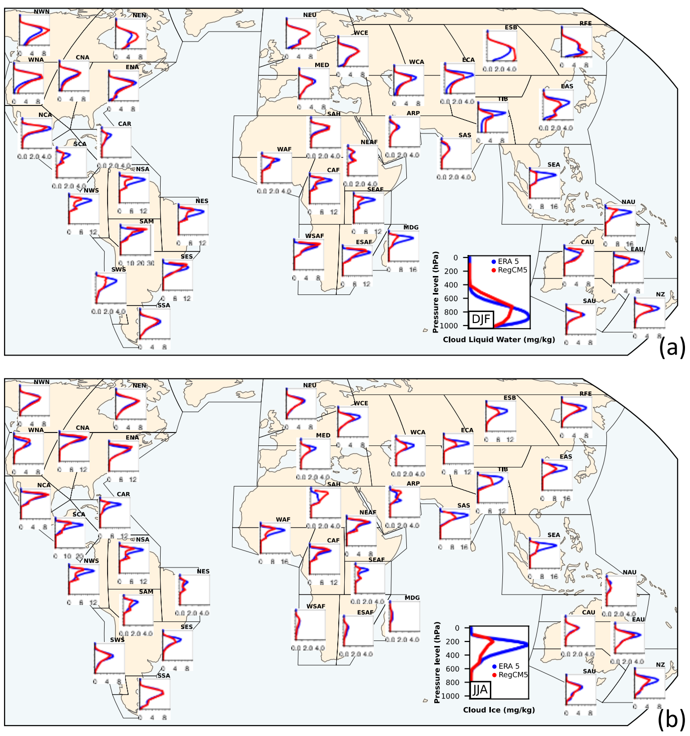

Figure S2: Cloud ice vertical profiles for DJF (a) and JJA (b). The period covered is 2000-2009, except for the European domain (MED, WCE and NEU regions): 1980-2010.

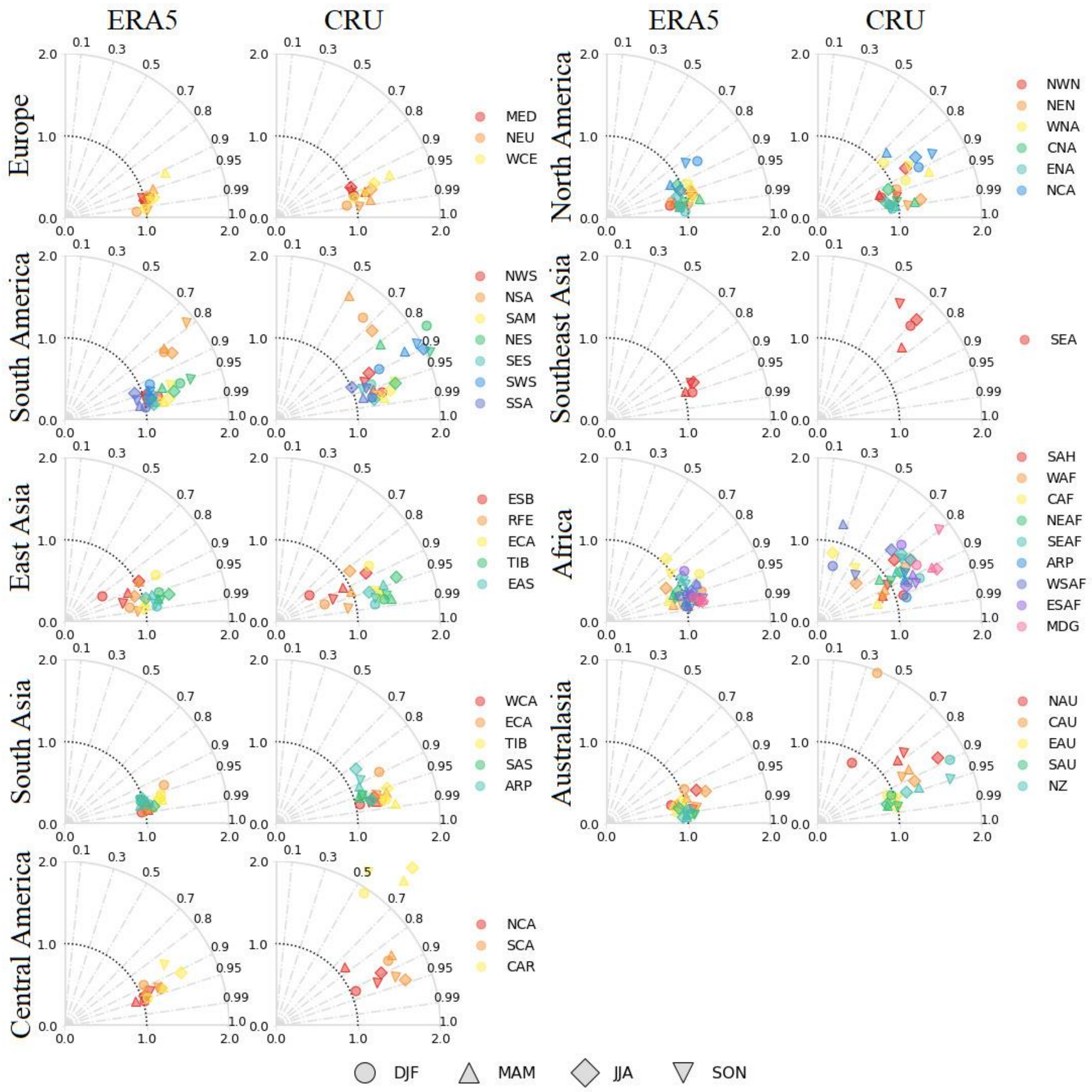

Figure S3: Taylor diagrams for the maximum temperature. Symbols represent seasons and colors are the subregions of a specific domain.

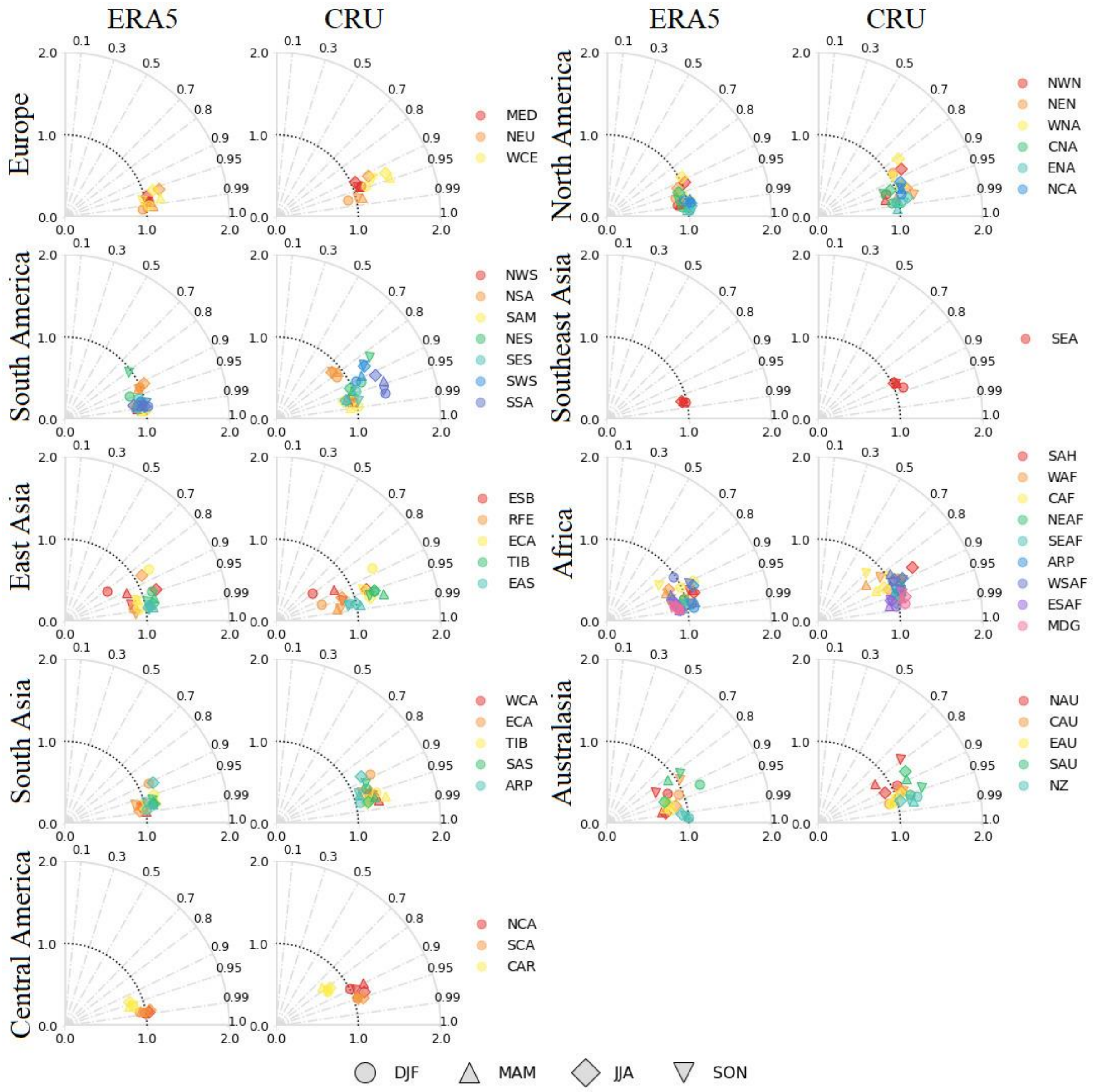

Figure S4: Taylor diagrams for the minimum temperature. Symbols represent seasons and colors are the subregions of a specific domain.

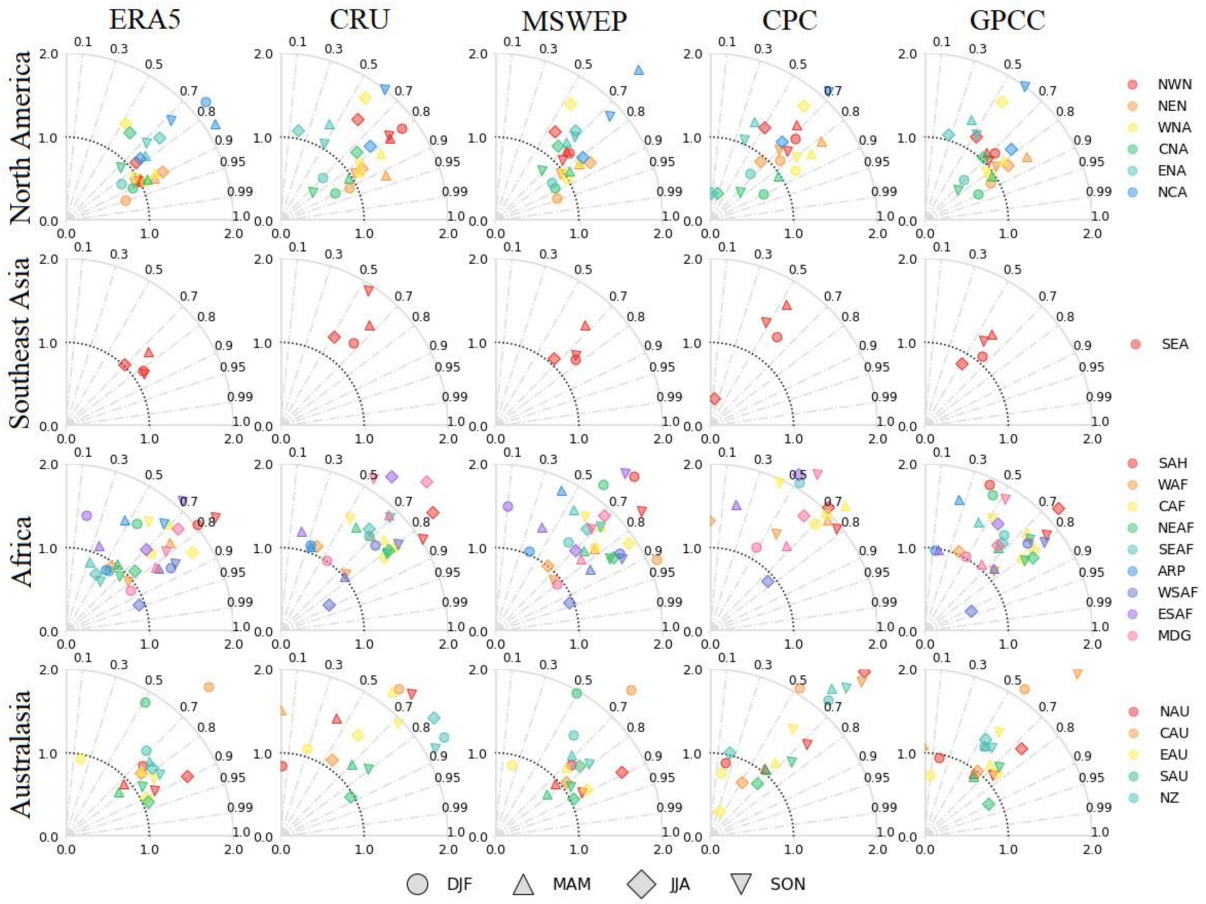

Figure S5: Taylor diagrams for precipitation for the remaining domains. Symbols represent seasons and colors are the subregions of a specific domain.

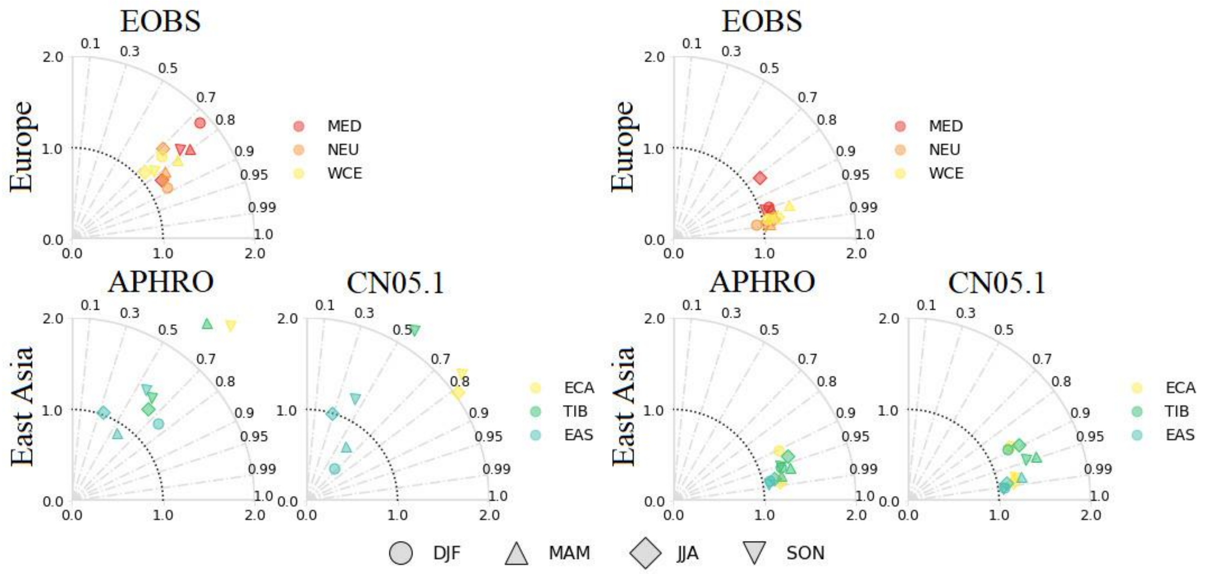

Figure S6: Taylor diagrams for precipitation (left panel) and temperature (right panel) with available regional datasets. (Note: For East Asia, results for RFE and ESB are not shown since APHORO and CN05.1 only cover a small portion of these subregions). Symbols represent seasons and colors are the subregions of a specific domain.

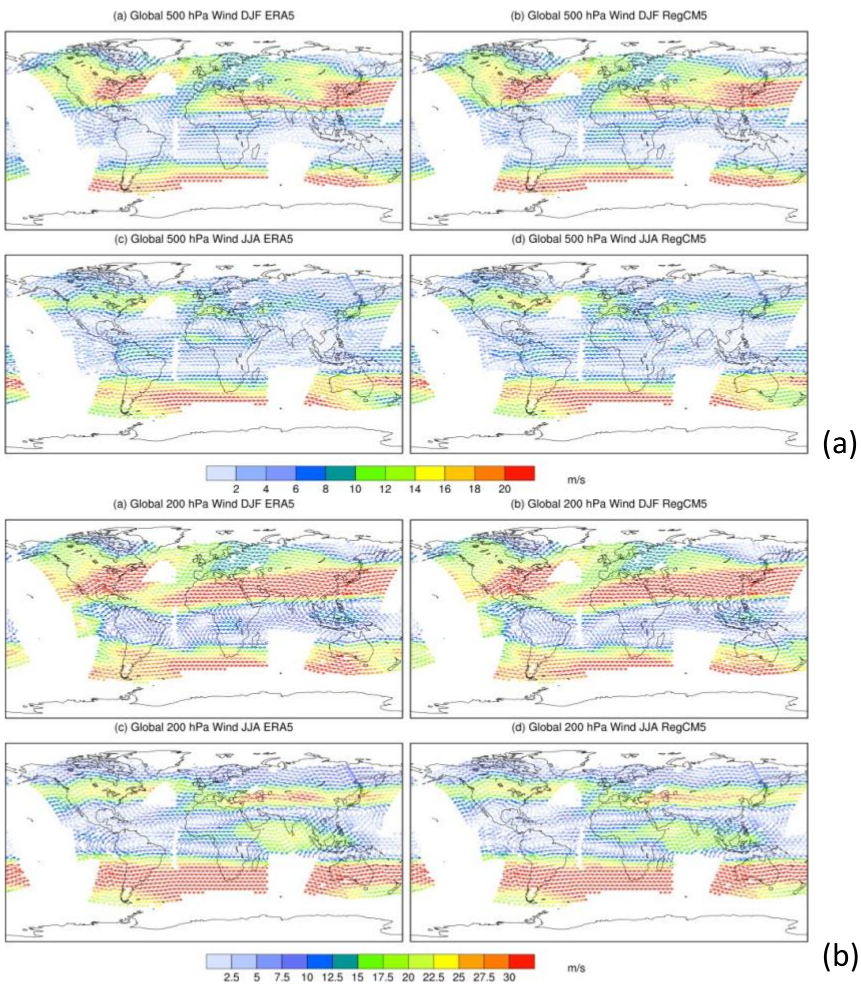

Figure S7: Wind field at 500 hPa (upper panel) and 200 hPa (lower panel).

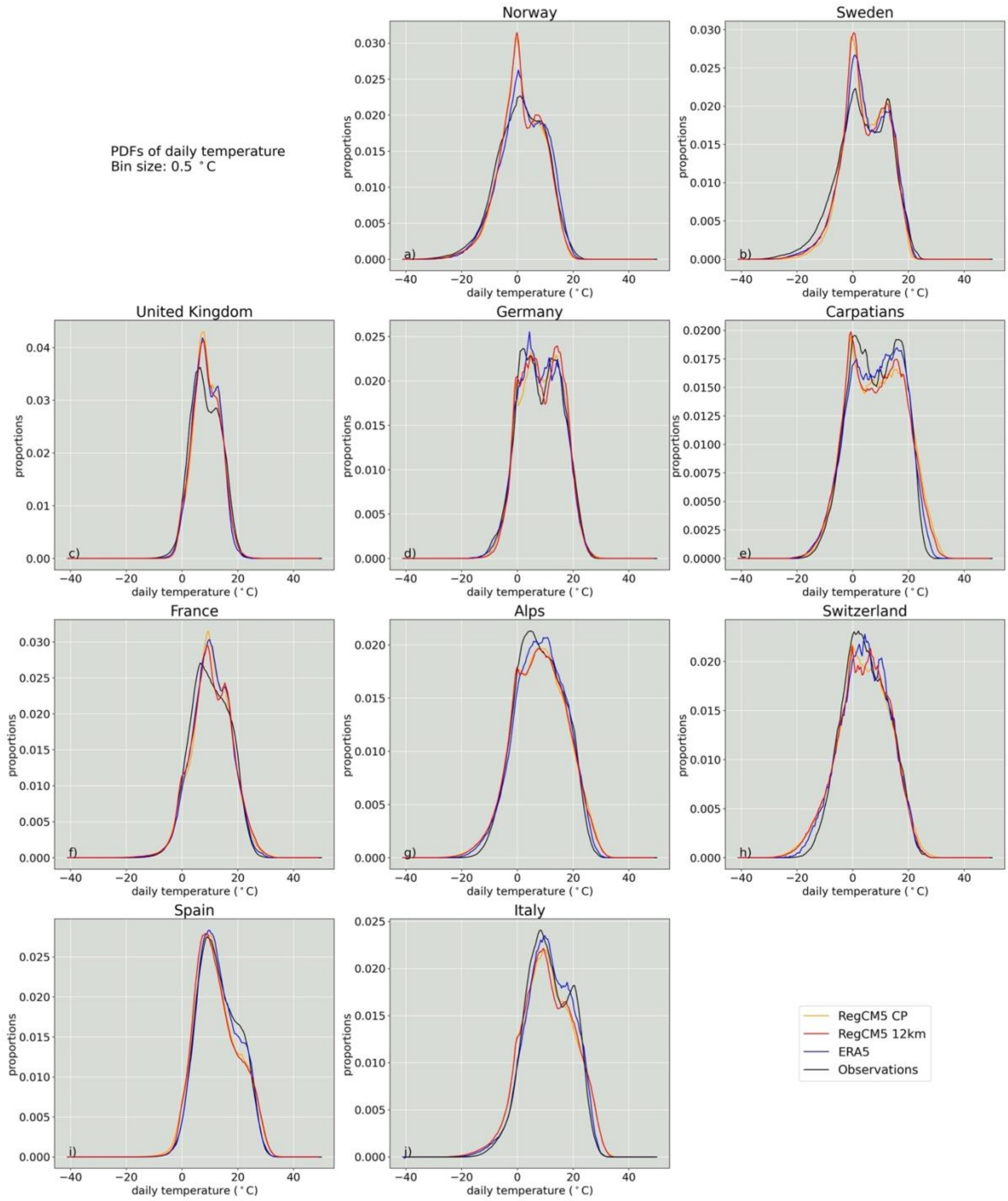

Figure S8: Probability density function distributions of the daily temperature [ºC] for the 10 regions investigated in the European domain. Each panel shows the distribution estimated from combining all available data for the years 2000-2004 for RegCM5 CP (orange), RegCM5 12km (red), ERA5 (blue) and observations (black). Details about the observational datasets for each region can be found in table 2.

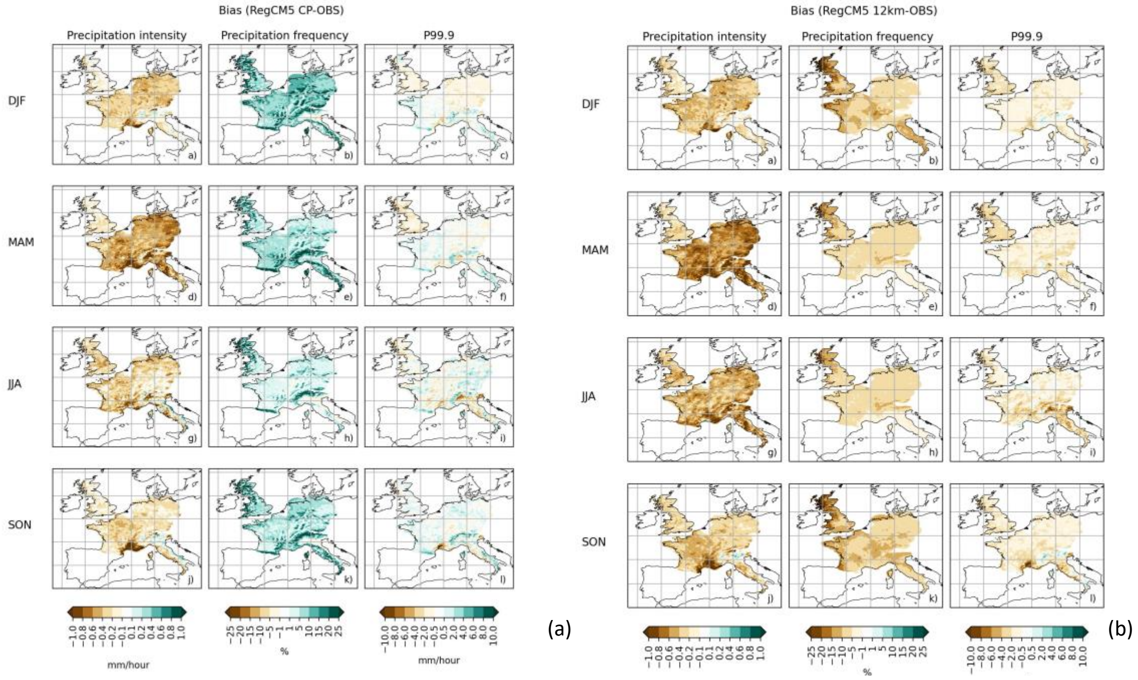

Figure S9: Precipitation intensity, wet frequency and P99.9 seasonal bias for hourly REGCM5 CP (panel a) and REGCM5 12km (panel b) versus high resolution observations. The seasonal biases are the same as in Figure 10, but using 0.1 mm/hr as threshold for the minimum precipitation in the REGCM5 simulations.

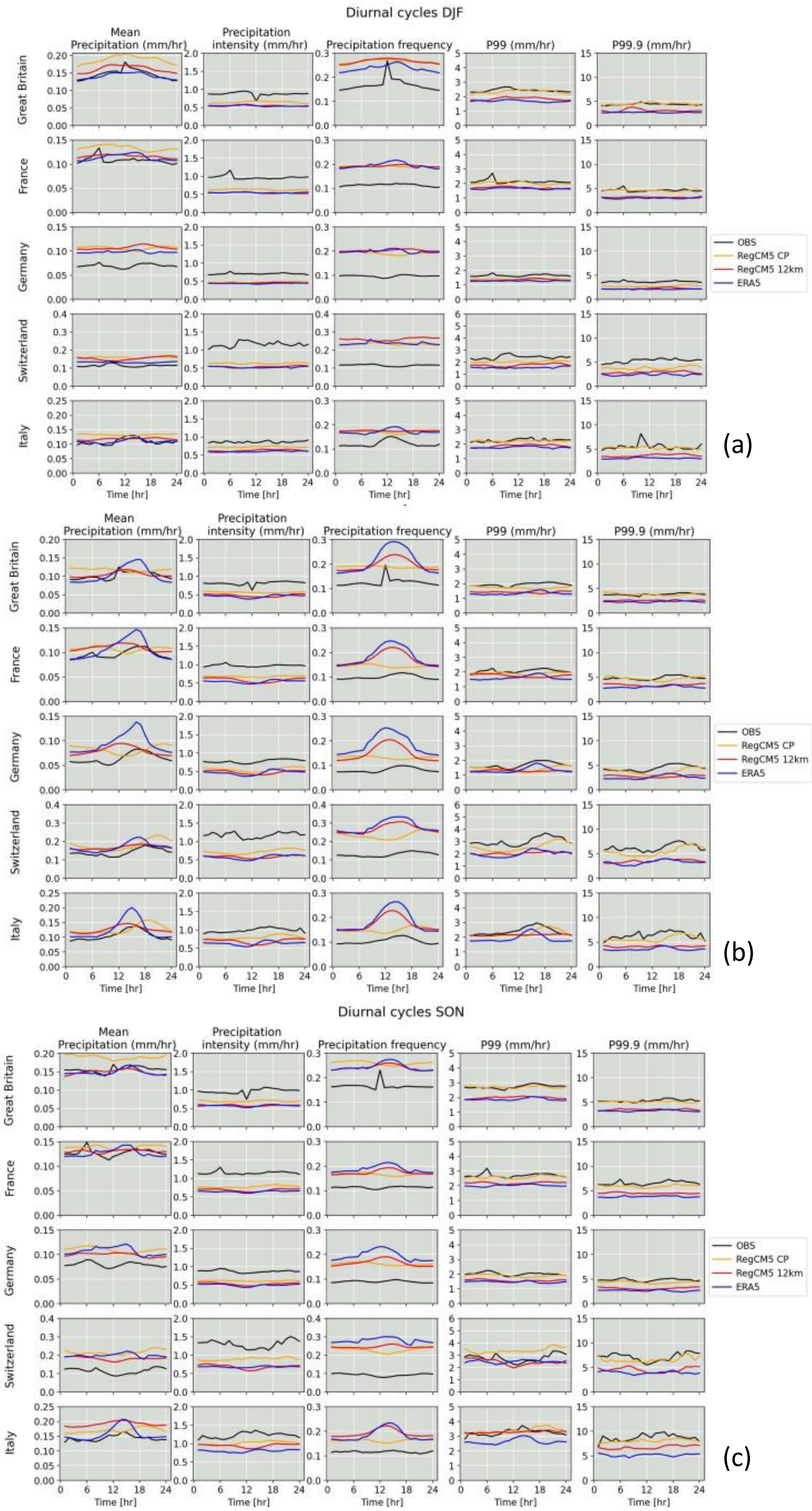

Figure S10: Diurnal cycles for mean precipitation (first column), precipitation intensity (second column), precipitation frequency (third column), p99 (fourth column) and p99.9 (fifth column) in DJF (panel a), MAM (panel b) and SON (panel c). In each panel, the results are shown for the following 5 regions in Europe: Great Britain (top row), France (second row), Germany (third row), Switzerland (fourth row) and Italy (bottom row).